TRANSIENT DISTRIBUTION OF REFRIGERANT AND OIL IN A RESIDENTIAL HEAT PUMP WATER HEATER SYSTEM

BY

WENZHE LI

THESIS

Submitted in partial fulfillment of the requirements
for the degree of Master of Science in Mechanical Engineering
in the Graduate College of the
University of Illinois at Urbana-Champaign, 2017

Urbana, Illinois

Adviser:

Professor Predrag S. Hrnjak

ABSTRACT

In most vapor-compression refrigeration systems, oil is added into the compressor for lubrication. However, it is inevitable that a portion of oil escapes from the compressor and circulates throughout the system due to the mutual solubility between the refrigerant and oil. The presence of circulating oil would affect the characteristics of heat transfer, pressure drop and mass retention in system. In addition, a large amount of retention of oil outside of the compressor might cause insufficient lubrication of the compressor, and eventually lead to compressor failure. The objective of this thesis is to experimentally and numerically investigate the transient refrigerant and oil distribution in a residential heat pump water heater (HPWH) system. In the experiments, R134a is used to pair with POE 22 oil as the working fluid. Quick Closing Valve Technique (QCVT) is employed to localize refrigerant and oil into each component of the system. Remove and Weigh Technique (RWT) is then used to measure the refrigerant mass, with an uncertainty about 0.17% of total refrigerant charge. The retained oil mass in each component, except for the compressor, is determined by Mix and Sample Technique (MST), of which the uncertainty is about 0.15% of total oil charge. Five experiments are conducted to cover a full heating process of five hours. The experimental data shows the retention of refrigerant is mainly determined by the internal volume and refrigerant density in the component. The retention of oil is found depending on the velocity of liquid refrigerant-oil mixture. A linked EES-CFD system model has been developed to simulate the transient system performance of the HPWH unit. Experimental data is used to validate this model. A retention model has also been established to analyze the local refrigerant and oil distribution in the heat exchangers.

ACKNOWLEDGEMENTS

This research project was funded by the Air Conditioning and Refrigeration Center (ACRC) in University of Illinois at Urbana-Champaign. Without the generous support of the ACRC members, this research would not have been possible. Special thanks go to the A.O Smith for providing the heat pump water heater unit and many valuable comments. I would like to deliver my sincere gratitude to my advisor, Professor Predrag S. Hrnjak for his support, guidance and encouragement. His passion and devotion towards this area would always inspire me. I want to thank Professor Fang Wang, for his help in the instrumentation of the experimental facility. I would also like to thank all my colleagues in ACRC for their selfless help and insightful suggestions. My gratitude goes to my parents for their unconditional support, care and love. Last but not least, special thank is given my girlfriend, Xi Liu for her accompany, trust and love which helps me went through all the tough and good days.

TABLE OF CONTENTS

LIST OF FIGURES

LIST OF TABLES

NOMENCLATURE

A	Area, m^2
AB	Alkyl benzene
A/C	Air conditioning
c	Oil concentration
c_p	Specific heat, kJ kg^{-1} K^{-1}
C	Heat capacity rate, kJ s^{-1} K^{-1}
C_r	Heat capacity ratio
COP	Coefficient of performance
D	Diameter, m
D_h	Hydraulic diameter, m
D_c	Collar diameter, m
EES	Engineering Equation Solver
EEV	Electronic Expansion Valve
f	Friction factor
F_p	Fin pitch, m
Fr	Froude number
g	Gravitational acceleration, m s^{-2}
G	Mass flux, kg m^{-2} s^{-1}
h	Enthalpy, kg kJ^{-1} or heat transfer coefficient, W m^{-2} K
j	Colburn factor
k	Conductivity, W m^{-1} K^{-1}
L	Length, m
$\dot{m}$	Mass flow rate, kg s^{-1}
M	Mass, kg
MO	Mineral Oil
MST	Mix and Sample Technique
MSD	Mix and Sample Device
NTU	Number of Transfer Unit
Nu	Nusselt number
OCR	Oil Circulation Rate
OLMT	On-Line Measurement Technique
OT	Orifice Tube
PAG	Polyalkelene glycol oil
PID	Proportional Integral Derivative
POE	Polyol ester oil
P	Pressure, kPa
Pr	Prandtl number
q''	Heat flux, W m^{-2}
Q	Heat exchanger capacity, kW
QCVT	Quick-Closing Valve Technique
Re	Reynolds number
RWT	Remove and Weigh Technique

t	Time, min
T	Temperature, ^{o}C or K
TXV	Thermal Expansion Valve
u	Velocity, m s^{-1} or uncertainty
U	Overall uncertainty or overall heat transfer coefficient, W m^{-2} K
V	Volume, m^3
$\dot{V}$	Volumetric flow rate
Vol	Element volume, m^3
W_{comp}	Compressor work, kW
W_m	Molecular mass, g mol^{-1}
x	Vapor quality
X_{tt}	Lockhart-Martinelli number

Greek Symbols

α	Void fraction
δ	Thickness, m
ε	Effectiveness or surface roughness, m
η	Efficiency
μ	Dynamic viscosity, Pa s^{-1}
ρ	Density, kg m^{-3}
σ	Surface tension, N m^{-1}
ϕ	Two-phase multiplier
ω	Refrigerant mass fraction

Subscripts

comp	Compressor
cond or c	Condenser
e	Element or evaporator
evap	Evaporator
i	Inlet
liq or l	Liquid
mix	Mixture
o	Outlet
ref or r	Refrigerant side
s	Isentropic
sat	Saturated
suc	Suction
v or vap	Vapor

CHAPTER 1-INTRODUCTION

1.1 Overview

In most vapor-compression refrigeration systems, oil is added into the compressor to lubricate its moving parts. It also severs as a sealing agent and/or a heat transfer medium for compressor cooling. However, due to the mutual solubility between the refrigerant and lubricant oil, it is inevitable that a portion of oil escapes from the compressor and circulates throughout the system. Depending on the location and system configuration, the oil appears in the system in forms of mist, droplets, oil-rich film or fairly homogeneous liquid mixture of refrigerant and oil. Generally, the presence of oil would change the thermal properties of the working fluid and deteriorate system performance by degrading heat transfer and increasing pressure drop. In addition, the retention of oil outside of the compressor might cause insufficient lubrication of the compressor, which would decrease the efficiency and reliability of the compressor. Therefore, the oil distribution or migration in the refrigeration system has a significant research value.

The oil distribution is highly related to the refrigerant distribution in the system because in most circumstances, the circulating oil tends to flow with the liquid refrigerant. In the heat exchangers, the concentration of oil in the liquid refrigerant-oil mixture significantly increases or decreases corresponding to the evaporation and condensation of refrigerant. Therefore, the study of refrigerant distribution is usually conducted simultaneously with the study of oil distribution. In addition, the exploration of refrigerant distribution in the system is in a great significance for another research topic: charge reduction or minimization. The location of refrigerant inventory actually reveals the potential of charge reduction in each component of the system.

There have been extensive literatures focusing on the refrigerant and oil distribution or migration in refrigeration systems. These studies aimed at different systems (residential/automotive systems; orifice tube/thermal expansion valve) and various operating conditions (cooling/heating; steady/ transients (stop/start)). Differentiating with the existing studies, this research targets the transient refrigerant and oil distribution in a residential heat pump water heater (HPWH) system during the heating process. The

unique coil structure of the condenser in the heat pump water heater has a relatively large height difference, which makes oil more likely to accumulate. The refrigerant and lubricant oil in this study are R134a and POE 22. Another objective of this study is to develop a reasonable model to predict the heating performance of this system, as well as the refrigerant and oil mass retention in heat exchangers.

1.2 Literature Review

1.2.1 Experimental methods to measure refrigerant distribution

In the literatures, the experimental methods of measuring refrigerant distribution can be divided into two main categories: the Quick-Closing Valve Technique (QCVT) and the On-Line Measurement Technique (OLMT). Both techniques obtain "refrigerant mass" directly. It should be noticed that besides these two methods, there are some other experimental techniques available in the literature which determine the refrigerant mass by locally measuring the void fraction via optical means, radioactive absorption scattering, or laser scattering [1]. The void fraction is the ratio of vapor refrigerant volume to the liquid refrigerant volume in a section. The application of these methods requires massive measurements of void fraction in every finite structure of each section, e.g., every channel in the heat exchanger, which is not feasible for the purpose of this research.

Quick-Closing Valve Technique (QCVT)

The Quick-Closing Valve Technique (QCVT) is an intrusive method since the system must be stopped when measuring the refrigerant retention. In QCVT, ball valves are installed at two ends of each section of interest. The refrigerant is trapped into each section by simultaneously closing all valves. The mass of the trapped refrigerant is then obtained by different secondary procedures. One commonly used way is called Remove and Weigh Technique (RWT) in which the refrigerant is recovered into a recovery cylinder by liquid nitrogen and the mass is the weight change of the cylinder before and after the recovery. Another method is to expand the refrigerant into a large vessel in which the superheat state is reached. Then the mass is calculated by the internal volume of the vessel and the pressure-volume-temperature (P-V-T) relationship [2].

In 1982, Tanaka et al [3] first applied the QCVT on a residential 1-ton R22 heat pump

system to explore the transient refrigerant migration during the start-up process. They used magnetic valves to divide the system into three sections: the indoor heat exchanger, the outdoor heat exchanger and the compressor section. An accumulator was also included into the compressor section. The Remove and Weigh Technique (RWT) was used to determine the mass of the trapped refrigerant in each section. After most of the refrigerant was recovered, the remaining refrigerant was assumed to be superheated vapor and the mass of which can be calculated by the internal volume and the vapor density based on the temperature and pressure measurements. The QCVT and RWT were also adopted by Mulroy and Didion [4] on a residential 3-ton R22 heat pump system running in cooling mode. They used five pneumatically operated valves to divide the system into five sections: the outdoor heat exchanger, the liquid line, the indoor heat exchanger, the vapor line and the compressor including the accumulator. Hoehne and Hrnjak [5] demonstrated in their experiments that, for a low charge (<150g) hydrocarbon (propane) system, less than 0.1 g of refrigerant would be left in the section if QCVT and RWT with liquid nitrogen cooling are used. Peuker and Hrnjak [6] used the same techniques (QCVT and RWT with liquid nitrogen cooling) to study the refrigerant migration in an automotive A/C system in steady and transient stop-start states. His data showed that the uncertainty of 0.4% regarding the total refrigerant mass was reached. On the same automotive A/C system as Peuker and Hrnjak [6], 2% deviation was observed by Jin and Hrnjak [7] with the same experimental procedures, when exploring the steady distribution of two different working fluids (R134a and R1234yf). Jiang and Hrnjak [8] used QCVT and RWT with liquid nitrogen cooling to seek the potential of refrigerant charge reduction in a typical bottle cooler. The error was within -9% for the total charge measurements in their five experiments.

The second method to determine the trapped mass of refrigerant was proposed by Björk [2]. In this method, a large expansion tank is used to accommodate the trapped refrigerant so that the superheat state is ensured. After the thermodynamic equilibrium is reached, the temperature and pressure are recorded. With the internal volume of the tank; the mass of refrigerant can be calculated using the P-V-T relationship. According to the Björk's comparison, the deviation between these two secondary procedures is ranging from

1%~5%.

On-Line Measurement Technique (OLMT)

Unlike the QCVT, the On-Line Measurement Technique (OLMT) is a nonintrusive means which allows a dynamic measurement of the refrigerant mass in a section without interrupting the operation. In this method, the section of interest is placed on a scale and its weight is directly measured while system is still running. Miller [9] applied this method to measure the migration of refrigerant entering or leaving the outdoor unit of a 3-ton R22 split-system air-to-air heat pump. The results showed that the accuracy of weighing system is about 0.05 kg. To eliminate the vertical thrust, Miller [9] used the flexible couplings between outdoor unit and the vapor/liquid line. Later, the OLMT was further developed by Belth et al. [10] to measure the dynamic mass change in each component of a 3-ton split-system air-to-air heat pump. Belth et al. [10] concluded that zigzag copper tubing around the component is necessary to reduce the stiffness of the refrigerant tubing. But this would significantly increase the refrigerant mass in the system.

1.2.2 Experimental results of refrigerant distribution

Tanaka et al [3] measured the refrigerant migration of a 1-ton R22 heat pump system in start-up, stop-start and steady state operation in three sections (compressor including the accumulator, indoor heat exchanger and outdoor heat exchanger). They found that at the steady state, 68.5% of the total refrigerant charge was found in the outdoor heat exchanger in cooling mode (as a condenser) and 35.7% in heating mode (as an evaporator). Mulroy and Didion [4] measured refrigerant distribution of a 3-ton R22 heat pump and found 83% of the total refrigerant charge was retained in the condenser and liquid line under steady state. They also concluded that during the start-up, the gradual release of liquid refrigerant held up in the accumulator into circulation attributed to much cyclic loss since the system was undercharged. By weighing the outdoor unit including the compressor, condenser and accumulator, Miller [9] measured the refrigerant distribution of a 3-ton R22 heat pump in heating mode for two different ambient temperatures. His experimental results showed that when the outdoor temperature increased from -1 ^{o}C to 10 ^{o}C, the refrigerant mass in the outdoor unit decreased from

53.7% to 34.2%. He concluded that, the extra mass was shifted into the accumulator. Belth et al. [10] measured the transient refrigerant migration during start-up and shut-down of a 3-ton R22 split-system air-to-air heat pump in cooling and heating mode. Their cooling mode results confirmed Mulroy and Didion's results [4]. They reported three major observations: first, very little refrigerant mass was found in the compressor; second, during the start-up, a large quantity of refrigerant shifted from the evaporator to the accumulator, and then the refrigerant slowly left the accumulator to join the circulation; last, during the shut-down, a large percentage of the refrigerant flowed back to the evaporator.

Hoehne and Hrnjak [5] obtained charge distribution data for an R290 (propane) refrigeration system under steady state conditions. Their results showed a relatively constant charge distribution with the cooling capacity held between 1.1 kW and 1.3 kW. The majority of the refrigerant mass (80%) was found in the compressor, condenser and evaporator in their experiments. Sheth and Newell [11] investigated a 1.5 kW R22 window air conditioning unit at steady state conditions. It was found for their particular system, the condenser has the largest internal volume, thus, the largest amount of oil and refrigerant was found in it out of all the components. Björk and Palm [12] reported their experimental results of steady state refrigerant distribution in a capillary tube cooling system at various thermal loads. They concluded that "condenser and compressor mass charges increased whereas the evaporator charge decreased upon increased thermal load". With thermal load increased from 74 W to 145 W in the tests, mass in the evaporator had the largest variation-an over 30% decrease. Björk and Palm [12] also indicated that the accumulator acted as a charge buffer which accommodated the refrigerant mass change of other parts in the system.

Peuker and Hrnjak [6] investigated lubricant and refrigerant migration during transients (stop/start) and steady state on a 4.2 kW R134a automotive A/C system. The system was divided into five sections: the compressor, condenser, liquid line, evaporator and accumulator. Refrigerant distribution was measured under different system charge: from "undercharge" (600g) to "overcharge" (1500g). The results showed that the mass of refrigerant in each component generally increased as total refrigerant charge increasing

before the critical charge (1000 g) was reached. However, after the critical charge, the increase in total refrigerant charge mostly went to the accumulator and the mass in other components remained fairly constant. Peuker and Hrnjak [6] also concluded that the refrigerant mass in the accumulator would be significantly underestimated if the effects of oil on the refrigerant thermal properties were not considered. Jin and Hrnjak [7] compared the steady refrigerant and oil distribution in two different automotive A/C systems: one with a fixed Orifice Tube (OT) and low pressure side accumulator, the other with a Thermal Expansion Valve (TXV) and a high pressure side receiver. Two different refrigerants (R134a and R1234yf) were used in experiments. Their data showed that in each system, R134a and R1234yf exhibited similar results in terms of refrigerant and lubricant retention at steady states. It was also observed that refrigerant retention in the same condenser of TXV system is significantly larger than that of OT system due to the higher subcooling of the TXV system. Jiang and Hrnjak [8] studied the refrigerant distribution in a typical bottle cooler to seek the potential of refrigerant charge reduction. They found that most of the charge is retained in the condenser and liquid line, while some portion of charge is in the evaporator and compressor. Based on experimental and modeling results, Jiang and Hrnjak [8] proposed that flattening the finless-round-tube of the heat exchanger to some proper extents is a simple way to reduce charge without penalizing system performance significantly.

1.2.3 Experimental methods to measure oil distribution

There have been extensive researches about the oil retention and/or oil circulation in the vapor-compression systems over past decades. Since the primary usage of oil is to lubricate the moving parts of compressor so that its durability and reliability is guaranteed, the terms “oil” and “lubricant” are often used interchangeably in literatures.

Various methods have been proposed to quantify the oil in different parts of the system. In 1997, Shedd and Newell [13] developed a nonintrusive, automated, optical technique to measure liquid film thickness. In this method, light is reflected from the surface of a liquid film flowing over a transparent wall. This reflected light generates an image on the outside of the wall. The positions of the reflected light rays can be calculated based on the pattern of this image. The film thickness and film slop can be thereby, calculated. Shedd

and Newell [13] reported this method gave the deviation within 2.2% comparing with the needle-contact method. In 2003, Lee [14] used injection-extraction method to investigate the oil retention in each component of a CO_2/PAG 46 A/C system. In this method, oil was injected at the inlet of a component and was separated at the outlet with an oil separator. The oil retention is obtained by measuring the differential oil volume between the injected oil volume and the oil volume extracted across the test section after steady state is reached. Later, Cremaschi [15] applied this technique on a residential A/C system in 2004. According to Cremaschi [15], the uncertainty of this method was estimated to be 12% relative error.

Peuker and Hrnjak [6] developed three secondary techniques after QCVT to investigate oil migration on an automotive A/C system under transients (stop/start) and steady state. Remove and Weigh Technique (RWT) was used to obtain the mass of oil contained in the compressor after refrigerant was recovered by liquid nitrogen. In this case, "Remove and Weigh" means physically remove a section from the system and compare the current weight to the tare weight. The oil retention in the accumulator was measure by flushing technique in which the accumulator was flushed by pure refrigerant for multiple times to remove all the oil out, and then weighed. For other components (the evaporator, condenser and liquid line), the Mix and Sample Technique (MST) was developed to quantify the oil retained. In MST, a known quantity of pure refrigerant is added into the section and fully mixed with the trapped oil. Then a small sample of well-mixed refrigerant-oil mixture is taken and the concentration of oil in the sample can be known by slowly releasing the refrigerant out. Thereby, the amount of oil trapped in the section can be obtained. This method was very time-consuming, but capable to determine a total amount of oil within 2% on a system with 4.2 kW cooling capacity, according to Peuker and Hrnjak [6]. Later, Jin and Hrnjak [7] used the same method to measure the lubricant distribution of two different automotive A/C systems. Their conclusions indicated the total mass of lubricant in the system was determined with 5% uncertainty in average.

1.2.4 Experimental results of oil distribution

Crompton et al [16] measured oil retention in smooth, axially microfinned and helically microfinned copper tubes. Several refrigerant/oil combinations have been tested include

R134a with a polyolester (POE), R134a with a polyalkylene glycol (PAG), R134a with an alkylbenzene (AB), R22 with an AB and R410A with a POE. In their experiments, oil retention was observed to be sensitive to quality, mass flux, tube type and lubricant concentration. Void fraction and flow visualization were examined to reflect the oil effect on flow patterns and a semi-empirical model was developed.

Lee [14] investigated the oil retention of a CO_2 A/C system. PAG 46 oil which is partially miscible with CO_2 was used in the experiments. It was found that increasing refrigerant mass flux would reduce the oil retention in the heat exchangers, and decrease the pressure drop penalty factor as well. An oil retention model was developed for the suction line under different conditions, which employed an empirical friction factor correlation.

Cremaschi [15] studied the oil retention in an A/C system with different refrigerant/oil mixtures: R22/ Mineral Oil (MO), R410A/POE, R134a/POE and R134a/PAG. Oil circulation rate (OCR) was found to have a significant impact on the oil retention in each component. Cremaschi [15] also concluded that the oil retained in the system would be reduced due to a lower liquid film viscosity, if the solubility and miscibility between the refrigerant and oil increases. Among the combinations investigated, R410A/MO mixtures showed the highest oil retention characteristics.

Peuker and Hrnjak [6] measured the migration of R134a and PAG 46 in an automotive A/C system. Under steady state condition, more than half (55%) of lubricant mass was found in the accumulator, 11% in the two heat exchangers and compressor and the rest in the liquid and discharge tube. With the total refrigerant charge exceeding the critical value (1000 g), more lubricant oil shifted to the accumulator and the oil retention of other components correspondingly decreased if the total oil supply kept unchanged. Additionally, an increase in total refrigerant charge was found decreased the OCR in system.

Jin and Hrnjak [7] compared the refrigerant and oil distribution in two different automotive A/C systems: one with a fixed Orifice Tube (OT) and low pressure side accumulator, the other with a Thermal Expansion Valve (TXV) and a high pressure side receiver. Two refrigerant/oil combinations (R134a/PAG 46 and R1234yf/PAG 46) were used in their experiments. They found that in OT system, oil concentration in each

component was generally higher when the system ran with R1234yf than R134a .Under similar OCR, TXV system had much higher oil retention in both heat exchangers due to higher condenser subcooling and evaporator superheat in the system.

1.3 Research Objective

The primary objective of this study is to investigate refrigerant and oil distribution in a residential heat pump water heater system. Emphasis goes to two unique features of this system: 1). The coil structure of the condenser in this heat pump water heater has a relatively large height difference, which makes oil more likely to accumulate; 2). The increase of water temperature makes the system in a transient state. R134a and POE 22 are used in this study. The method of Quick Closing Valve Technique (QCVT) is used to localize working fluid into several sections at different time points in the heating process. Different secondary techniques are applied to obtain the quantity of the trapped refrigerant and oil. An EES-CFD linked model is to be developed to predict heating performance of this unit. The refrigerant and oil retention in two heat exchangers is also to be predicted numerically.

CHAPTER 2-EXPERIMENTAL SYSTEM

2.1 Experimental Facility

The experimental facility used in this study is instrumented on the base of a residential heat pump water heater (HPWH) unit, which contains an evaporator, a low-pressure side accumulator, a compressor, an electronic expansion valve (EEV), a wrap-around coil condenser, and a water tank. The schematic of the experimental facility is given in Figure 2.1. R134a and POE 22 are used in this system. The evaporator is a fin-and-tube heat exchanger and a fan is installed at the back of this evaporator to drive the air flow to provide heat to this heat pump system. A back pressure reciprocating compressor, in which the shell (where lubricant oil stored) is at the suction gas pressure, is used in this system. The condenser has two parallel aluminum coil tubes which are wrapped around the wall of a stainless steel water tank of 66 gallon capacity. For a better contact with the tank wall, the coil tubes are designed to have a D-shaped cross section.

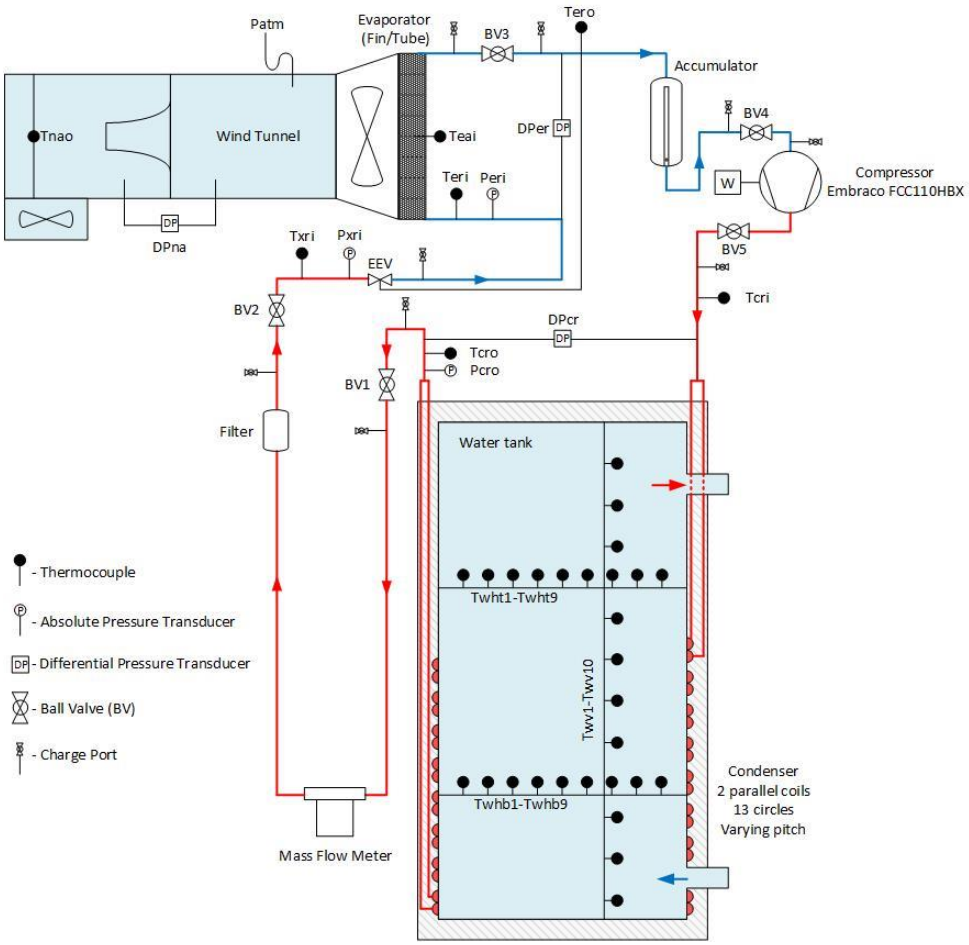

Figure 2.1 Schematic of experimental facility

The original design for this particular HPWH contains two immersed electric resistance heaters that operate in lieu of the heat pump system when demand or temperature difference exceeds ability of the heat pump to supply hot water adequately. For the purpose of this study, the electric heaters have been removed, and the heating of water only relies on the vapor-compression system.

In addition to these major components from the original heat pump system, type-T immersed thermocouples and absolute pressure transducers are installed to measure temperature and pressure at several key locations in the refrigeration loop to monitor the states of refrigerant. Two differential pressure transducers are also used to measure the pressure drop across the evaporator and condenser. A Coriolis type mass flow meter, installed in the liquid line where fluid is in a subcooled single phase, is used to measure total mass flow rate. A wattmeter is connected to the compressor to record the power consumption.

To implement the QCVT in this system, 5 manually operated ball valves are installed into the refrigerant loop, which divide the system into 5 sections: the condenser, liquid line, evaporator, accumulator and compressor. To be clarified, the liquid line in the original HPWH system is much shorter than its current length. It has been artificially prolonged to accommodate the space needed for mass flow meter. Two charge ports are also added at two ends of each section for the secondary procedures of refrigerant/oil retention measurements.

In the air side, a wind tunnel is used to obtain the air side energy balance. By measuring the pressure difference of air flow through a nozzle in the wind tunnel, the air flow velocity can be calculated. There is a blower at one of the wind tunnel used to compensate the extra flow resistance introduced by the nozzle. By adjusting the opening at the end of the wind tunnel, the atmospheric pressure can be achieved right after the evaporator. By this means, the influence of the wind tunnel on the evaporator could be eliminated. Type T welded thermocouple wires are mounted in front of the evaporator and at end of the wind tunnel to obtain air side temperature change.

In the water side, 28 thermocouples are put in the water tank to monitor the temperature change during the heating process, 10 of them are placed vertically with 5.08 cm (2 inch)

interval; rest 18 are placed horizontally at two levels: 27 cm and 76.1 cm above the bottom respectively. Each horizontal series has 9 thermocouples with 5.08 cm (2 inch) interval.

The data acquisition system consists of a datalogger (21X Micrologger) and two relay multiplexers with 16 channels each. Data is acquired and sent to Excel with an adjustable time interval. The data is then processed in Engineering Equation Solver (EES) [17] and Excel.

The entire experimental facility is placed in an environmental chamber where a PID-controlled heater is used to provide the required heat of this HPWH system and maintain the ambient temperature of the chamber relatively constant.

2.2 Data Reduction and Uncertainty

Following equations are used to evaluate the heating performance of this HPWH system based on the direct measured variables in the experiments.

In the refrigerant side, the enthalpy of single-phase refrigerant flow at a certain location can be determined by the temperature and pressure:

$$h_{single-phase} = f(T, P) \tag{2.1}$$

The functions between enthalpy and temperature and pressure are built in EES [17]. Refrigerant at inlet/outlet of the condenser, outlet of the evaporator, before the expansion valve should be single phase, thus the equation (2.1) can be used. Since the throttling process is regarded as isenthalpic, therefore:

$$h_{eri} = h_{xri} \tag{2.2}$$

The capacity of two heat exchangers can be calculated by the enthalpy difference between the inlet and out:

$$Q_{cond} = \dot{m}_{ref} \cdot (h_{cri} - h_{cro}) \tag{2.3}$$

$$Q_{evap} = \dot{m}_{ref} \cdot (h_{ero} - h_{eri}) \tag{2.4}$$

Therefore, the COP of this system is given by the ratio between condenser capacity and power of compressor:

$$COP = \frac{Q_{cond}}{W_{comp}} \tag{2.5}$$

Table 2.1 lists the measurement instruments and their specifications.

The uncertainty of direct measurements is also given in Table 2.1. The error propagation rule, given in equation (2.6) is used to estimate the overall uncertainty based on uncertainties of the directly measurements.

$$u_c = \sqrt{\sum_{i=1}^{N} \left(\frac{\partial y}{\partial x_i}\right)^2 u^2(x_i)} \tag{2.6}$$

Where, u_c is combined uncertainty, y is calculated variable, x_i is a directly measured variable and $u(x_i)$ is the uncertainty of x_i. An expanded uncertainty interval U, with a factor of 2, is chosen for a higher level of confidence of approximately 95%, according to the normal distribution function.

$$U = 2 \cdot u_c \tag{2.7}$$

Thus, the calculated variable Y, can be expressed as:

$$Y = y \pm U \tag{2.8}$$

Table 2.1 Specifications of experimental instruments

Instruments	Range	Accuracy	Description/Location
Type T welded thermocouple wire	-200 ℃ to +200 ℃	0.1 ℃ (Calibrated)	air/water temperatures
Type T immersed thermocouple	-200 ℃ to +200 ℃	0.1 ℃ (Calibrated)	refrigerant temperatures
Absolute pressure transducers	0 to 3548.7 kPa 0 to 3447.4 kPa 0 to 3447.4 kPa	±0.25 % full scale ±0.1 % full scale ±0.05 % full scale	Condenser outlet Evaporator inlet EEV inlet
Differential pressure transducers	0 to 103.4 kPa 0 to 103.4 kPa 0 to 622.7 Pa	±0.1 % full scale ±0.1 % full scale ±0.073 % full scale	DP of condenser DP of evaporator DP of nozzle (air)
Mass flowmeter	0 to 29.19 g/s	±0.15 % of flow rate	Refrigerant mass flow rate
Wattmeter	0 to 4 kW	±0.2 % of reading	Compressor power

Table 2.1 (cont.)

Instruments	Range	Accuracy	Description/Location
Scales	0 to 8200 g 0 to 15 kg	±0.1 g ±0.5 g	Sample cylinder; Compressor and refrigerant cylinder

2.3 Measurement of Internal Volume

It is very crucial to know the internal volume of each section since it directly indicates how much physical space the section has to contain refrigerant/oil. Two methods are applied to determine the internal volume of each section: Liquid Refrigerant Method and Isothermal Gas (CO_2) Method.

Liquid Refrigerant Method

In this method, each section would be fully filled with the subcooled liquid refrigerant after the evacuation of oil and air. The quantity of liquid refrigerant used can be obtained by the weight difference of refrigerant source cylinder before and after the liquid refrigerant is consumed. To guarantee the subcooled state of refrigerant in each section, the source cylinder will be heated to a relatively higher temperature, so that the possible vapor generated in charging process would condense into liquid again due to the lower ambient temperature. After the thermodynamic equilibrium is reached in the section (this usually takes several hours depending on the internal volume of the section), the temperature and pressure data is recorded to calculate the density of subcooled liquid refrigerant, and then, with the mass of refrigerant, the internal volume is known.

Isothermal Gas (CO_2) Method

The basic principle of the isothermal gas method is quite similar to the liquid refrigerant method. Each section is filled with a known amount of gas. Density is calculated based on equilibrium temperature and pressure. Volume is thus calculated as the ratio of mass and density. Gas with higher density is preferred because the scale would have a better accuracy if the weight difference is large. Carbon dioxide (CO_2), with a stated purity of 99.9% as received, is used. To avoid dissolve of carbon dioxide into the lubricant, oil, as

well as air, must be removed from the system before charging. The procedure is repeated twice for each section

The measurement results are given in Figure 2.2, for each method, the procedure is repeated twice for each section and the average values are taken. The internal volumes obtained using two methods agree well with each other (deviation < 5%), thus the average values of these two methods are used. Compared with the data from the manufacturer, the system internal volume is enlarged due to the installation of the sensors and valves.

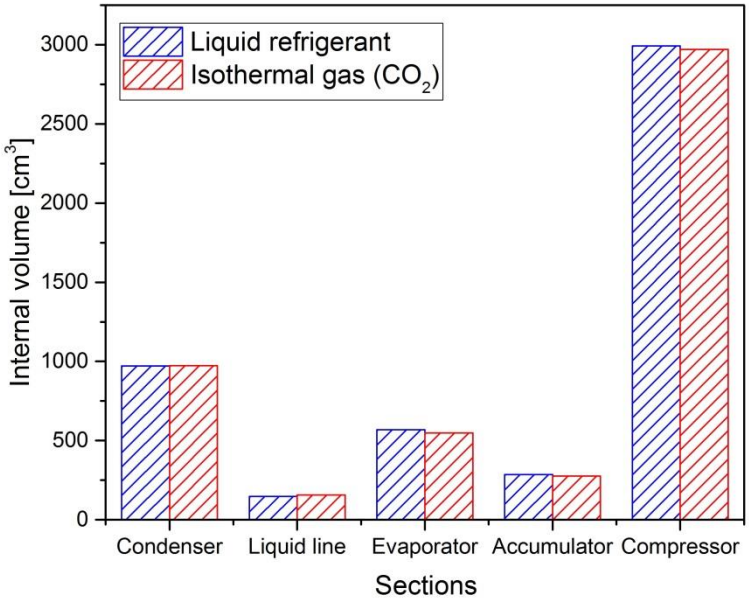

Figure 2.2 Measurements of internal volume by two methods show a good repeatability

2.4 System Flushing

There are two reasons for system flushing: 1) As it is mentioned above, the measurement of internal volume requires no oil in each section; 2) It is hard to determine how much oil the system contains after each experiment, so that all oil in the system other than in the compressor, needs to be removed and oil should be recharged to a desired quantity. Besides, for the compressor, RWT is employed to obtain the oil quantity in it, in which the tare weight of compressor is also needed.

A commercial recycling device, Robinar 700, is used to flush all sections except compressor. It fills the section with R134a and pumps liquid refrigerant circulating throughout the entire section. Exploiting the miscibility of POE 22 and R134a, this

machine uses liquid refrigerant to absorb oil and then drain oil into oil bottle after separation. According to Jin and Hrnjak [7], three times flushing should be enough for the components other than compressor.

This recycling device could not be applied on the compressor since the piston of compressor has very tight seals which would block the circulation of liquid refrigerant. The compressor must be flushed manually by filling liquid R134a to dilute the oil. During the flushing, the compressor is waggled gently to help oil dissolving. Then refrigerant-oil mixture is drained through a side process port of the compressor. The weight of the compressor (vacuumed but with oil), is recorded after each flushing. The flushing will be continued until the difference of compressor weight between two flushing is smaller than the detection limit of the scale (0.5 g). Figure 2.3 shows the compressor weight after each flushing. The weight of compressor stabilizes after 9 time flushing and this weight can be taken as the tare weight of the compressor.

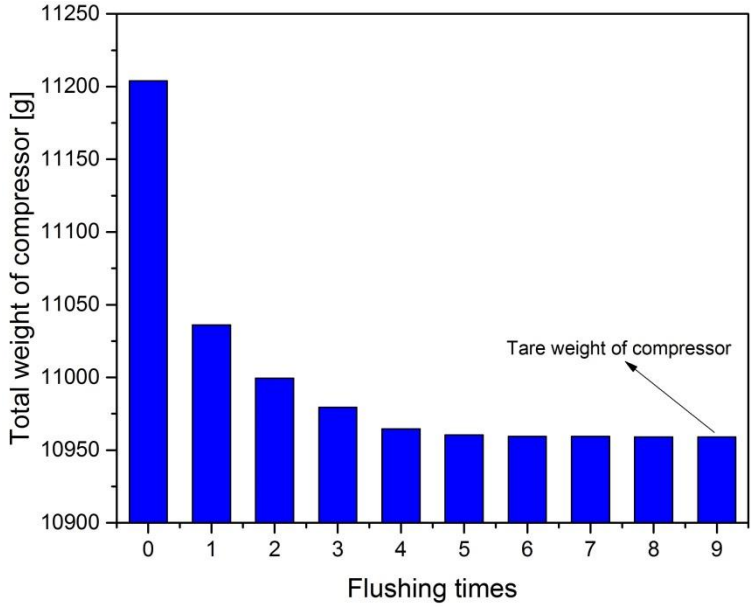

Figure 2.3 Compressor weight changes indicate all oil was removed after the ninth flushing

Before the first experiment, the nominal charge of oil (273.5 g) is added into the suction housing of the compressor through the process port. After each experiment, extra oil will be supplied to the compressor to maintain the nominal charge at the beginning of the next experiment.

CHAPTER 3-EXPERIMENTAL METHODS AND PROCEDURES

Peuker and Hrnjak [6] concluded that Quick Closing Valve Technique (QCVT) is the more suitable for the objective of this study, which is to measure the transient refrigerant and oil distribution in the major components of a residential heat pump water heater system. Several secondary techniques have been developed by Peuker and Hrnjak [6] and Jin and Hrnjak [7] to obtain the quantities of the trapped refrigerant and oil in each section after QCVT is applied, and some of them are also used in this study. The mass of refrigerant in each section is obtained by the Remove and Weigh Technique (RWT) with liquid nitrogen recovery. Oil retention in each section, except for compressor, is measured by the Mix and Sample Technique. For oil in the compressor, Remove and Weigh Technique (RWT) is applied once again but with different procedure: physically take out the compressor from the system, evacuate the refrigerant dissolved in oil, and compare its current weight with the tare weight of the compressor.

3.1 Procedure for Measuring Refrigerant Distribution

Quick Closing Valve Technique (QCVT) is used to localize the refrigerant and oil over the system. 5 ball valves divide the entire HPWH system into 5 sections: the condenser, liquid line, evaporator, accumulator and compressor. At different time points during the heating process, by simultaneously closing these 5 valves, the refrigerant and oil will be trapped into each section. The ball valves require a quarter turn to be fully closed and they are operated manually by 5 college-age students under the stimuli of sound. This would introduce some error due to the non-simultaneity of valve closing, which would be analyzed later in this chapter. The system is shut down right after the valves are closed.

Remove and Weigh Technique is then applied to measure the mass of refrigerant retained in each section. In this method, sampling cylinder, which is cooled with liquid nitrogen, is connected to the charge port of the section through low-loss refrigerant hoses. After evacuation, slowly open the valve on the charge port to control the recovery speed and avoid too much oil entering the cylinder. Wait until the pressure in the section decreases to a relatively stable value (<20 kPa), then disconnect the cylinder and warm it up above

the dew point temperature and measure its weight. It is unavoidable that a small amount of oil entering the sampling cylinder, thus the measured weight includes both refrigerant and oil.

To separate refrigerant from oil, the sampling cylinder is connected to an ice-bathed recovery cylinder through a volumetric flow meter. By controlling the flow rate, vapor refrigerant is slowly recovered. After the pressure difference between the sampling cylinder and ice-bathed cylinder disappears (no flow can be maintained), the sampling cylinder is immersed into hot water and vacuumed for 20 min. Only oil is left in the sampling cylinder at this time and it is weighed again. With the tare weight of sampling cylinder, total weight of cylinder and refrigerant-oil mixture and weight of cylinder and oil, the mass of refrigerant and oil can be obtained respectively. After that, all oil in the sampling cylinder would be removed by acetone. The sampling cylinder would be weighed again after evacuation, to ensure the same tare weight is obtained. Two verification tests have been conducted to prove that under a certain flow rate, oil would not be taken out by the refrigerant vapor. In these tests, a certain quantity of oil and refrigerant were added in a sampling cylinder. Followed the procedure described above to separate refrigerant and oil and then compared the oil mass obtained with the original oil mass. Two different refrigerant/oil ratios have been used (518 g/25.9 g and 547 g/5.4 g) and under the tested flow rate, no oil was lost. Therefore, the tested flow rate is controlled as the max flow rate in the separation.

After above procedures, the majority of refrigerant in the section has been recovered. But, there is still a small portion of refrigerant dissolved in the oil and released over time. According to Peuker and Hrnjak [6], it takes over 12 hours for this part of refrigerant to be fully released and the system reaches equilibrium. Therefore, the system is left at rest for at least 12 hours and then the equilibrium temperature and pressure is recorded to obtain the vapor density. Along with the internal volume of the section, the mass of remaining refrigerant can be known.

When applying this method to the compressor, one more procedure is needed. Because the compressor contains a large quantity of oil, relatively more refrigerant is dissolved in oil and it may not be fully released after 12 hours' resting. So that, the compressor would

be taken out from the system, and vacuumed for a short period of time to evacuate the air. The vacuum is stopped as long as the pressure inside the compressor stabilizes at a relatively low value (< 5 kPa). Then it is weighted for the first time. Continue vacuuming until the weight of the compressor stabilizes. Now, there is only oil left in the compressor. The difference between the first weight and the last weight is mass of refrigerant dissolved in oil.

3.2 Procedure for Measuring Oil Distribution

Remove and Weigh Technique (RWT) is only applied to measure the oil retained in the compressor. As described above (section 3.1), the compressor has been physically removed from the system and all refrigerant has been extracted. The difference between the weight after evacuation and the tare weight of the compressor is the mass of lubricant.

To measure retained mass of oil in other sections (condenser, evaporator, liquid line and accumulator), the Mix and Sample Technique (MST) is used. The MST was developed by Peuker and Hrnjak [6]. Jin and Hrnjak [7] also applied this method in their exploration of oil migration in an automotive A/C system. The basic ideal behind this technique is to mix the retained oil with a known quantity of refrigerant and take a sample of the homogeneous refrigerant-oil mixture. Measuring the concentration of oil in the sample, the quantity of retained oil is then determined by the sampled oil concentration and the mass of pure refrigerant infused. The Mix and Sample Device (MSD), shown in Figure 2.1, is designed to homogenize the refrigerant-oil mixture. In this device, a gear pump drives the refrigerant-oil mixture circulating throughout the connected section and device, a mixing vessel provides a space for fully mixing and a side transparent side tube is used to monitor the liquid level. The MSD, mounted on a portable frame, is installed at a higher elevation than the sections. After the MSD is connected with a target section and vacuumed, hot pure refrigerant is charged through the charge port until the liquid level is close to the top of the transparent tube but a small amount of vapor is still visible. The higher elevation of the MSD and hot refrigerant could guarantee the section is fully filled with liquid refrigerant and eliminate possible vapor packets during charging. The quantity of refrigerant charge is determined by the weight difference of the refrigerant source tank.

Then, the gear pump, driven by magnetic force to avoid introducing another lubricant, is turned on for at least 1 hour. To take a sample, a sampling cylinder is connected to the MSD and immersed into liquid nitrogen in a container. Liquid nitrogen provides a vacuuming effect due to the fact that at the liquid nitrogen temperature under the atmospheric pressure of -195.8 ^{o}C, the vapor pressure of R134a is near to 0 kPa. The valve before the sampling cylinder is then slowly opened, and another transparent tube after the valve is used to avoid possible flashing during the sampling. The quantity of sampling is monitored and controlled by the side transparent tube. After sampling, the weight of refrigerant and oil in the sampling cylinder are determined by the methods described above.

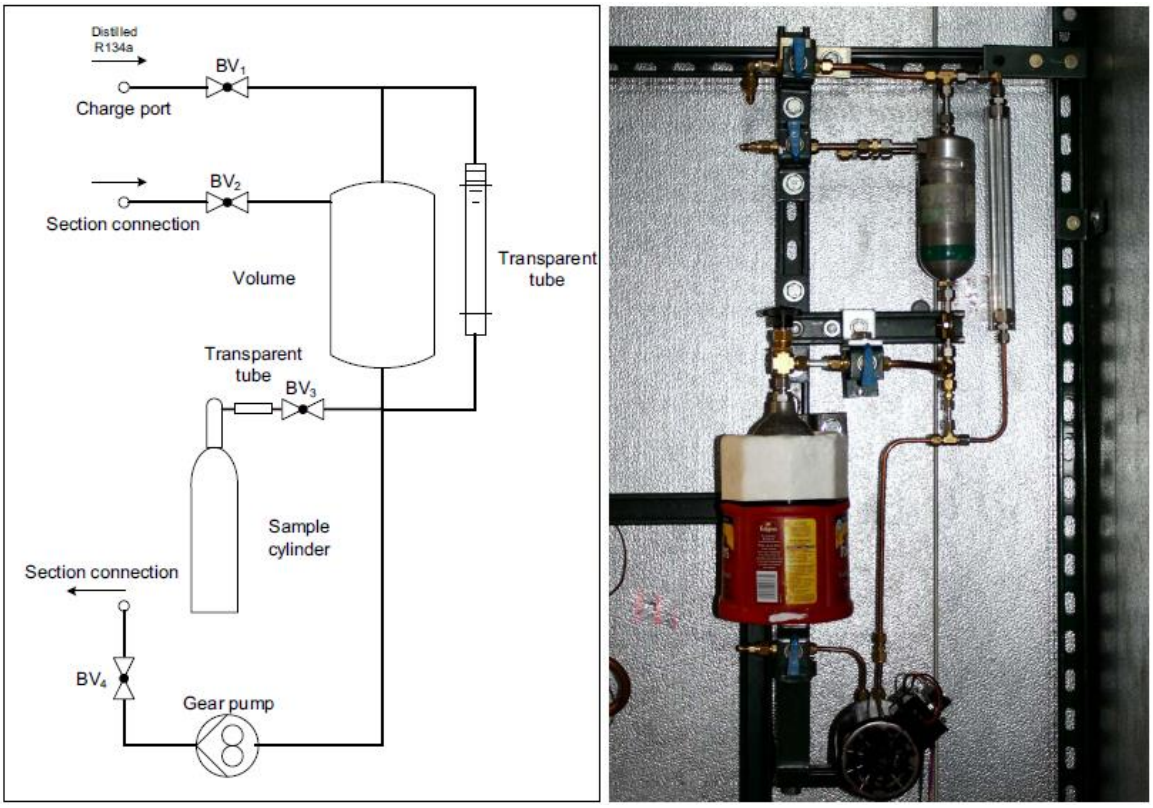

Figure 3.1 Schematic and picture of Mix and Sample Device, adapted from [6]

Ideally, the concentration of oil in the mixture of the section and the sampling cylinder should be equal and following equation could be established:

$$c_{oil,section} = \frac{M_{oil,section}}{M_{oil,section} + M_{ref,charge}} = c_{oil,sample} = \frac{M_{oil,sample}}{M_{oil,sample} + M_{ref,}} \quad (3.1)$$

However, two corrections need to be considered in Equation (3.1). The first one accounts

the inactive volume between the ball valve 3 and the tee junction below the mixing vessel. The liquid refrigerant in this volume does not participate the circulating or mixing, but enters the sampling cylinder. The mass of the refrigerant in the volume is

$$M_{ref,tube} = \rho_{ref,liq-sat} \cdot V_{tube} \tag{3.2}$$

Here, $\rho_{ref,liq-sat}$ is the saturated liquid density of refrigerant and V_{tube} is the inactive volume. This part of "inactive" mass must be subtracted from the total mass in the sampling cylinder since it does not contain any oil.

$$c_{oil,sample} = \frac{M_{oil,sample}}{M_{oil,sample} + M_{ref,sample} - M_{ref,tube}} \tag{3.3}$$

Another correction is considering that during the sampling process, the volume originally occupied by the sampled liquid would be filled with evaporated vapor refrigerant. This would increase the concentration of oil in liquid mixture. To correct this, first express this part of volume in following way:

$$V_{sample} = \frac{M_{ref,sample}}{\rho_{ref,liq-sat}} = \frac{M_{ref,vapor}}{\rho_{ref,vap-sat}} \tag{3.4}$$

The initial oil concentration in the section can be given by

$$c_{oil,initial} = \frac{M_{oil,section}}{M_{oil,section} + M_{ref,charge} - M_{ref,tube}} \tag{3.5}$$

After sampling process, the final oil concentration in the section is

$$c_{oil,final} = \frac{M_{oil,section} - M_{oil,sample}}{M_{oil,section} + M_{ref,charge} - M_{ref,tube} - M_{ref,sample} - M_{ref,vapor}} \tag{3.6}$$

The representative oil concentration in the section during the sampling process is taken as the average of the initial and final concentration

$$c_{oil,section} = \frac{c_{oil,initial} + c_{oil,final}}{2} \tag{3.7}$$

And it is equal to the oil concentration in sampling cylinder

$$c_{oil,section} = c_{oil,sample} \tag{3.8}$$

The mass of oil retained in the section can be calculated by solving Equation (3.2) to (3.8) together.

To test the accuracy of the Mix and Sample Technique (MST), several verification experiments have been conducted. In these experiments, a known quantity of oil is

charged into a vessel to simulate the oil retained in a section. Then, the MST is applied to obtain the oil quantity in the vessel, and the measured oil mass is then compared with the original charge. Five tests have been conducted to cover a possible range of oil retention in reality. The results are given in Figure 3.2. Within the tested range, the deviation between the charged oil mass and measured oil mass is less than 0.4 g. Overall, it can be concluded that the MST is capable to measure the oil retention in the section with an acceptable accuracy. And 0.4 g is taken as the uncertainty of the MST.

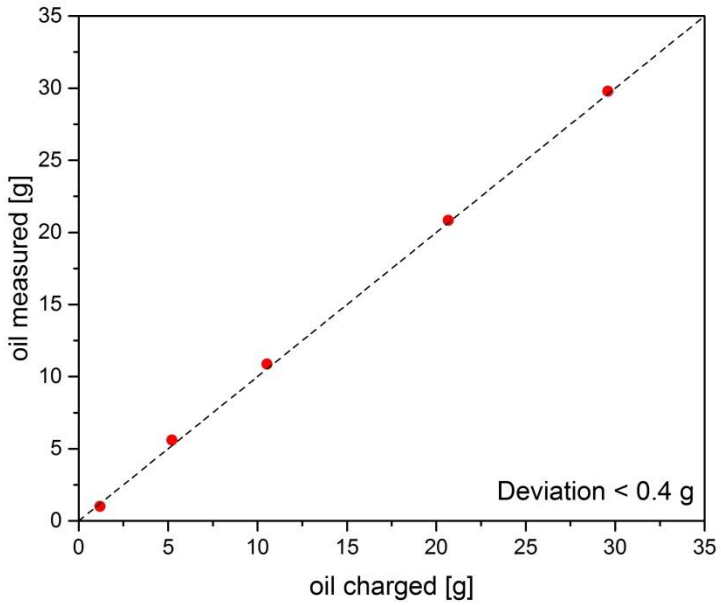

Figure 3.2 Verification tests of the Mix and Sample Technique (MST)

3.3 Sources of Uncertainty

There are two major sources of uncertainty in the measurements of refrigerant and oil distribution.

First is the uncertainty of instrumentation listed in Table 2.1. Among them, the accuracy of scale directly influences the results of mass retention. The uncertainties of temperature, pressure and mass flow rate measurements, in general, would mainly affect the uncertainty of system performance. However, the results of refrigerant retention would also be affected since it involves equilibrium temperature and pressure measurements. The error propagation rule discussed in 2.2 is used to estimate overall uncertainty caused by instrumentation.

Second is the uncertainty of simultaneousness of closing the valves. In QCVT, 5

valves are operated manually under sound stimuli. Brebner and Welford [18] indicated that the average reaction time for college-age individuals exposed to sound stimuli is 0.16 s. The uncertainty of closing valves is thus determined as follows.

$$U_{ref} = \dot{m}_{total} \cdot \Delta t \cdot (1 - OCR) \tag{3.9}$$

$$U_{oil} = \dot{m}_{total} \cdot \Delta t \cdot OCR \tag{3.10}$$

For the uncertainty of refrigerant retention measurements, the uncertainty of closing valves makes the major contribution to the overall uncertainty. For the uncertainty of oil retention measurements, the uncertainty of closing valves can be negligible because of low OCR, and the uncertainty of MST (0.4 g, described above) is used as the overall uncertainty.

In this study, five experiments have been conducted to measure the refrigerant and oil distribution after HPWH running for 1~5 hours. For each experiment, the refrigerant and oil retention in all five sections have been determined by the methods and procedures described above. After each experiment, the system would be cleaned by the flushing machine and recharged to a desired amount of refrigerant and oil. Therefore, the difference between the original charge of refrigerant and oil, and the summation of measured refrigerant and oil in each section is an indication of overall measurement uncertainty. The results are shown in Figure 3.3. The higher deviations in the refrigerant mass than oil mass can be seen in Figure 3.3. This is because the charge of refrigerant (≈ 813.5 g) is much higher than the charge of oil (≈ 273.5 g). From the aspect of the relative value, it can be concluded that the deviation in refrigerant or oil mass is less than 0.7%.

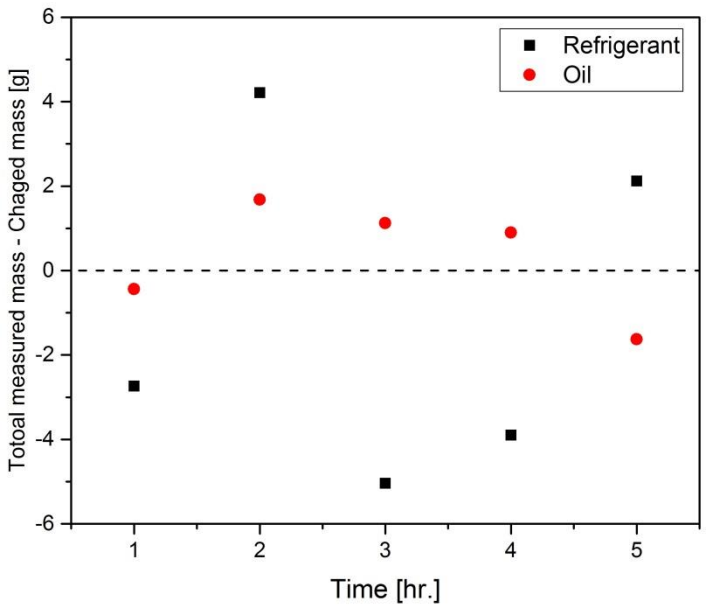

Figure 3.3 Comparison of total measured mass and initial charge

CHAPTER 4-EXPERIMENTAL RESULTS

4.1 Charge Determination

The refrigerant charge is one of the main factors affecting system performance. In industry, the optimal charge is often determined by charging the system until the cooling/heating capacity reaches its maximum. This simplifies the test procedure since only measurements (temperature and flow rate) in air side are needed. In this study, the optimal charge is selected to maximize the Coefficient of Performance (COP), so it is named "COP maximizing change". The experimental system starts with a low charge, and runs a full heating test, and then a small amount of refrigerant is added into the system to run the next test. For each test, the water tank is fully filled with water at an initial temperature of 25 ^{o}C. No water would be added in or drain out from the tank during the test. The air side temperature is fixed at 25 ^{o}C. This condition is also used in the study of refrigerant and oil migration later. Typically, a full heating test lasts for 5 hours to heat water from 25 ^{o}C to about 50 ^{o}C. Data is recorded very 30 s. Since the water temperature increases with the time, the test is actually under a transient condition. Therefore, an average COP of 5~300 minutes is used to compare the different refrigerant charges. The exclusion of the data before 5 minutes is to rule out the influence of start-up process. The changes of the heating capacity and COP with different refrigerant charge in HPWH system are plot in Figure 4.1

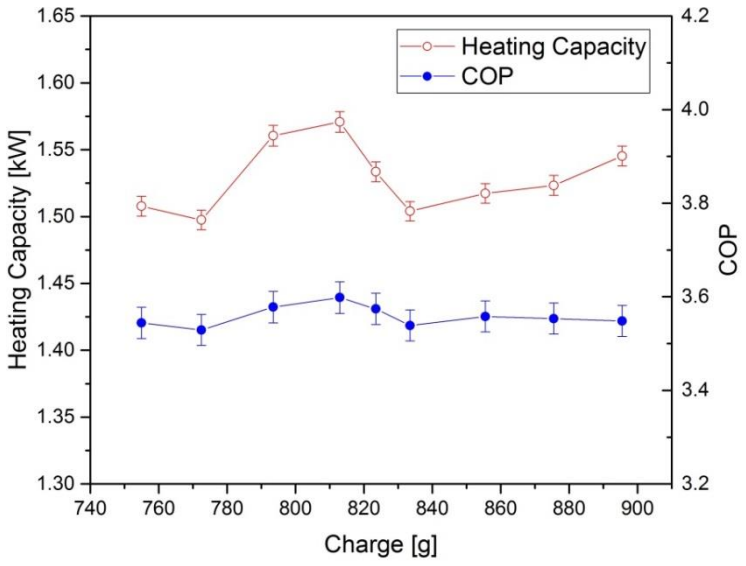

Figure 4.1 Charge determination tests

Figure 4.1 shows both the heating capacity and COP reach their maximum value with the refrigerant charge around 813.5 g. Therefore, 813.5 g is selected as the COP maximizing charge for this system. This charge is maintained during the later study of refrigerant and oil migration.

The nominal charge of this system is 735 g, which is less than the COP maximizing charge obtained above. This may be because the internal volume of the tested system is larger than the original system due to the installation of sensors and valves.

4.2 Heating Performance

As described above, this HPWH unit takes 5 hours to heat a full tank of water from an initial temperature of 25 ^{o}C to about 50 ^{o}C. No water is drain from the tank during the heating. The ambient temperature is fixed at 25 ^{o}C. Data is taken at a time interval of 30 s during the heating tests. The heating performance of this HPWH is then analyzed.

Figure 4.2 gives the changes of capacities and COP with respect to the time. Although the data is recoded every 30 s, the curves in Figure 4.2 is plotted with the data of 5 minutes interval for a better representation. It is clear in the Figure 4.2, the capacity of two heat exchangers, as well as COP, generally decreases with the time. This is because the water temperature increases in time, which increases the temperature difference between the heat sink and heat source, degrading the cycle efficiency.

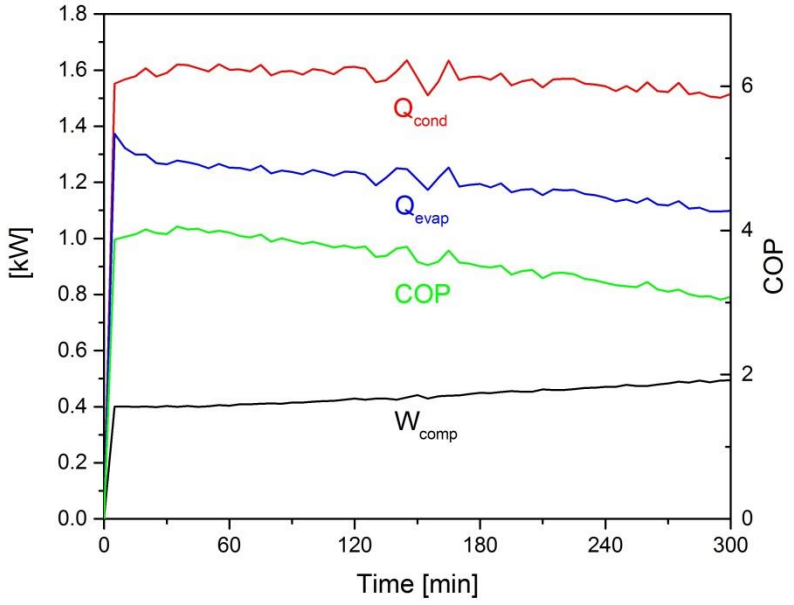

Figure 4.2 Main performances of the HPWH examined in the test with initial water temperature at 25^{O}C, air temperature at 25^{O}C

The P-h diagram of the heating process is given in Figure 4.3. Generally, the condensation pressure (temperature) increases with the time to respond the increase in water temperature. The elevation in condensation pressure also generates a higher subcooling because of a steeper liquid-phase line of R134a. With the constraint of ambient temperature, there's no too much variation in evaporation pressure (temperature). However, the inlet quality of the evaporator increases with the time. The superheat is controlled at a relatively constant value by Electronic Expansion Valve (EEV).

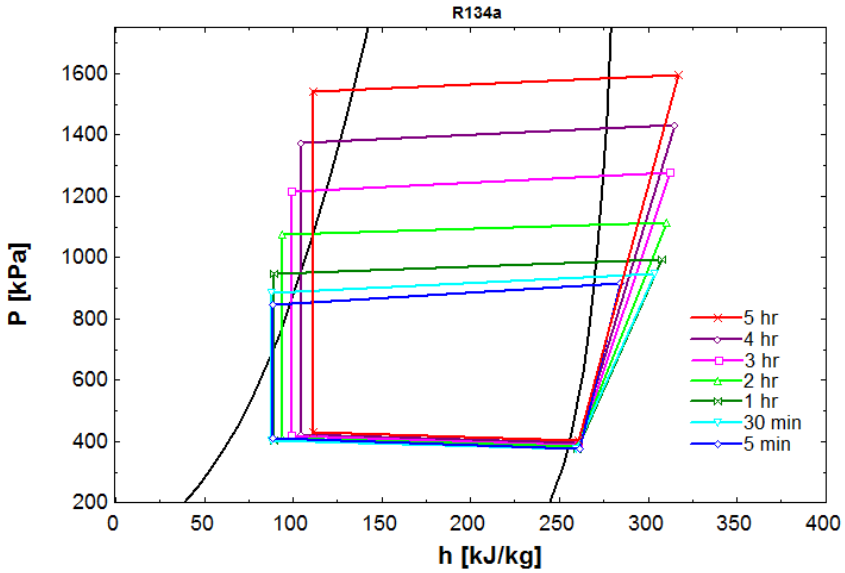

Figure 4.3 Development of the operating condition of the system: little change of the evaporation temperature is due to constant ambient conditions while pressure increase in the condenser is due to warming of the water in the tank

In the experiments, three series of thermocouples are put in the water tank: 10 vertically placed with 5.08 cm interval; 18 horizontally placed at two levels: 27 cm and 76.1 cm above the tank bottom. The average temperatures of these three thermocouple series are also given in Figure 4.4.

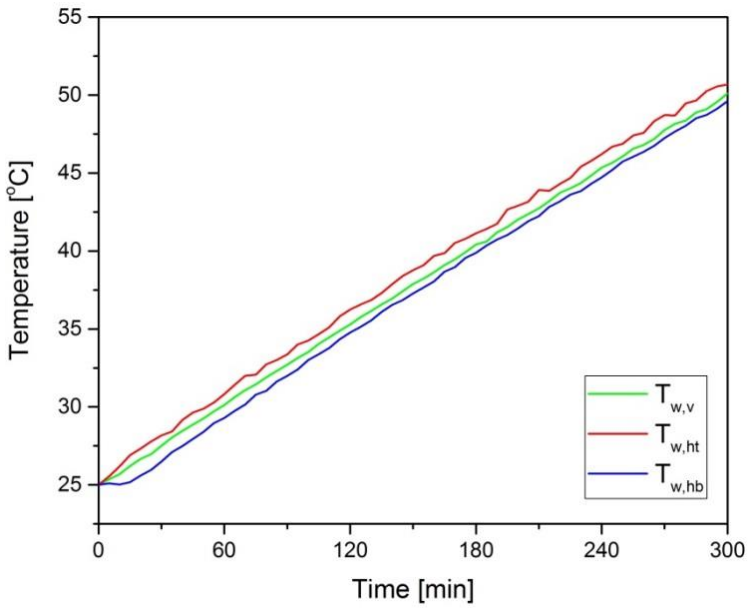

Figure 4.4 Development of water temperature during five hours' heating of the tank

Here, $T_{w,v}$ denotes the average temperature of the vertical series; $T_{w,ht}$ and $T_{w,hb}$ denote the top and bottom horizontal series respectively. The difference among these three temperatures reflects the stratification of the water temperature. This is important since the density difference caused by the temperature difference is the driving force of natural convection in the water tank, which would affect system performance.

4.3 Distribution of Refrigerant Mass in System

As discussed before, five experiments have been conducted to explore the transient distribution of refrigerant and oil with the system running for 1~5 hours. The initial water temperature and ambient temperature are kept unchanged. In an ideal case, the charge of refrigerant and oil should be the same in these experiments. However, it is very hard to charge the system with an exact same quantity of refrigerant or oil in subsequent experiment. In this study, the deviation in the refrigerant charge is less than 6 g, and in the oil charge, it's less than 3 g. To eliminate the influence of unequal charge, the results of refrigerant and oil distribution are presented by percentage.

The transient refrigerant distribution is shown in Figure 4.5. It can be seen in the Figure 4.5 that the refrigerant distributions among 5 sections are quite similar at different time points (1~5 hours). Generally speaking, the condenser has the highest refrigerant retention (≈60%) due to its relatively large internal volume and a moderate average

density of two-phase refrigerant. Liquid line has the smallest internal volume among all 5 sections, but it retains the second largest refrigerant mass (≈20%) due to a heavy density of liquid refrigerant in it. It's worth noticing that this liquid line section does not exist in the original HPWH unit, which means this part of refrigerant can be taken out in a real commercial product. The evaporator has a moderate internal volume and two-phase refrigerant density, which makes about 14% of refrigerant retained in it. Although the compressor has the largest internal space, only less than 7% of total refrigerant is found in it. This is because the majority of the compressor internal volume is occupied by the superheated vapor refrigerant. But there is still a portion of refrigerant dissolved in the oil, and reserves as the refrigerant-oil mixture in the compressor. Accumulator is found to have the smallest amount of refrigerant in 5 sections. This means under the selected charge, the accumulator is not used as storage of refrigerant, but functions as a separator.

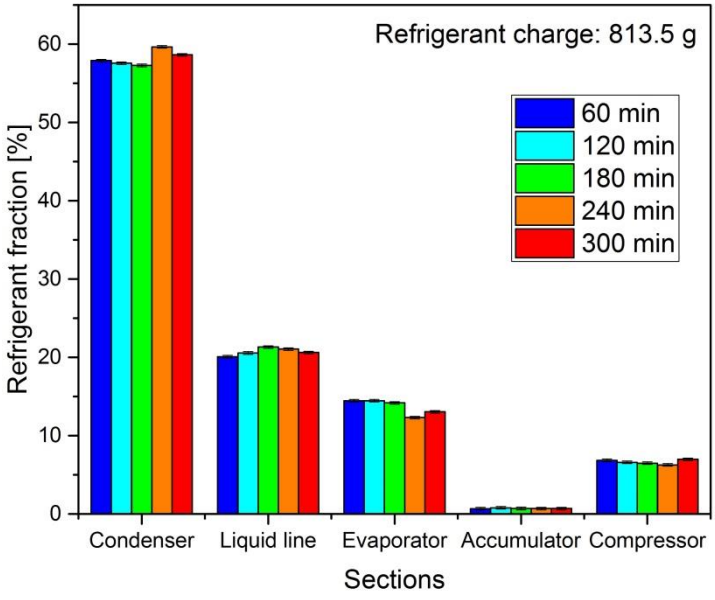

Figure 4.5 Distribution of refrigerant in five experiments show a high similarity and insignificant migration of refrigerant in time

Figure 4.5 also reveals the transient migration of refrigerant among 5 sections in 5 hours' heating. It seems that the refrigerant retention in liquid line, accumulator and compressor keeps a relatively constant value during the heating process. This is because the refrigerant is almost single-phase in these three sections, and the densities (subcooled liquid and superheated vapor) do not change too much during the heating. Phase change occurs in two heat exchangers. In the evaporator, the refrigerant generally decreases with

the time. This is because the inlet quality of the evaporator increases with the time (see P-h diagram in Figure 4.3) and that makes more internal volume is occupied by vapor refrigerant. On the contrary, the condenser holds an increased refrigerant mass with time. Actually, it can be observe in the Figure 4.3, with the elevation of the condensation pressure, the superheated region and subcooled region are both increasing with time. Obviously, the increasing refrigerant retention is dominated by the increase in subcooled region, instead of the increase in superheated region.

Based on the data in Figure 4.5, as well as the pressure and temperature measurements during the tests and the internal volume, the average liquid fraction in each section can be calculated. The liquid fraction is defined as the ration of liquid occupied volume to the total internal volume. In each section, the measured refrigerant mass can be expressed as the sum of liquid refrigerant and vapor refrigerant in Equation (4.1).

$$\left[\rho_{vap} \cdot \alpha + \rho_{liq} \cdot (1-\alpha)\right] \cdot V = M_{ref,section} \tag{4.1}$$

Here, α is the average void fraction of the section. The densities in Equation (4.1) are approximated by the saturated vapor and liquid density of the refrigerant at the average pressure.

$$\rho_{vap} \approx \rho_{sat,vap}(P_{avg});\ \rho_{liq} \approx \rho_{sat,liq}(P_{avg}) \tag{4.2}$$

The average liquid fraction in each section can be calculated by solving Equation (4.1) and (4.2). The results are shown in Figure 4.6. As described above, the refrigerant in the liquid line, accumulator and compressor is almost single-phase and that is also reflected in Figure 4.5. The liquid fraction of these sections is either 100% (liquid line) or near 0% (accumulator and compressor). For both heat exchangers, the trend of liquid fraction accords with the trend of refrigerant retention. In the condenser, the liquid fraction increases with time, while in the evaporator, it decreases.

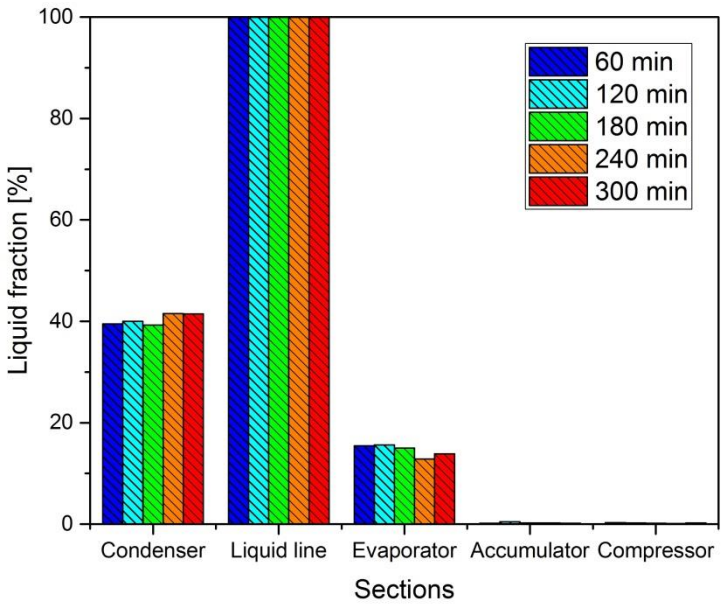

Figure 4.6 Average liquid fraction (1- α) of local refrigerant distribution

To further analyze the refrigerant retention in two heat exchangers, the liquid and vapor refrigerant distribution at 1~5 hours have been estimated by Equation (4.3) and (4.4) below, and given in Table 4.1. The results are also presented by percentage.

$$\rho_{vap} \cdot \alpha \cdot V = M_{ref,vap} \tag{4.3}$$

$$\rho_{liq} \cdot (1-\alpha) \cdot V = M_{ref,liq} \tag{4.4}$$

According to the estimation in Table 4.1, for the evaporator, the vapor refrigerant increases and liquid refrigerant decreases with the time. This agrees with two previous observations: the inlet quality increases and the average liquid fraction decreases with the time. For the condenser, it seems that its vapor refrigerant mass also increases with time. This might be because a higher vapor density at a higher condensation pressure compensates the decrease in void fraction (see Figure 4.5). The liquid refrigerant mass in the condenser is estimated to first decrease then increase with the time. This may be the outcome of compromise between the increasing liquid fraction and a varying liquid density.

The estimation in Table 4.1 is very rough due to the usage of saturated densities to represent the actual densities. More detailed analysis using finite element method is discussed in Chapter 6.

Table 4.1 Estimated liquid and vapor refrigerant distribution in heat exchangers

Time [min]	Condenser		Evaporator	
	$M_{ref,vap}$ [%]	$M_{ref,liq}$ [%]	$M_{ref,vap}$ [%]	$M_{ref,liq}$ [%]
60	3.39	54.52	1.02	13.46
120	3.72	53.86	1.02	13.45
180	4.41	52.87	1.06	13.13
240	4.68	54.98	1.08	11.23
300	5.24	53.40	1.09	11.98

4.4 Distribution of Oil Mass in System

Table 4.2 shows the oil distribution with the HPWH system running for 1~5 hours. The results are also given in percentage of the initial total charge. It can be seen that the most of oil still stays in the compressor during the 5 hours' heating. Only less than 4% of oil escapes from the compressor. The escaped oil is mainly distributed in two heat exchangers and the accumulator. A very small portion of oil (< 0.2%) is found in the liquid line. With the refrigerant and oil retention in the liquid line, the system OCR (Oil Circulation Rate) at different time points can be calculated. The calculated OCR for this HPWH system is ranging from 0.25% to 0.29%.

To analyze the transient migration of oil in the system, a bar graph, shown in Figure 4.7, is used to present the data in Table 4.2, but the oil retention in the compressor is excluded due to its large scale. It can be clearly seen from the Figure 4.7 that, during the heating, the evaporator holds more and more oil. But for the condenser, the oil retention seems to decrease at the beginning, and later increase. Both the refrigerant and oil mass in the liquid line are relatively constant during the heating process, and that leads to an almost constant system OCR. The accumulator serves as a separator to avoid liquid refrigerant entering the compressor. Its complex geometry may contribute to an irregular change of retained oil mass in the accumulator.

Table 4.2 Distribution of oil [%]

Time [hr.]	Condenser	Liquid line	Evaporator	Accumulator	Compressor
60	1.38	0.17	0.89	0.91	96.65
120	1.28	0.16	0.99	0.87	96.70
180	0.99	0.17	1.00	0.96	96.88
240	1.10	0.17	1.21	0.73	96.79
300	1.28	0.16	1.31	0.92	96.33

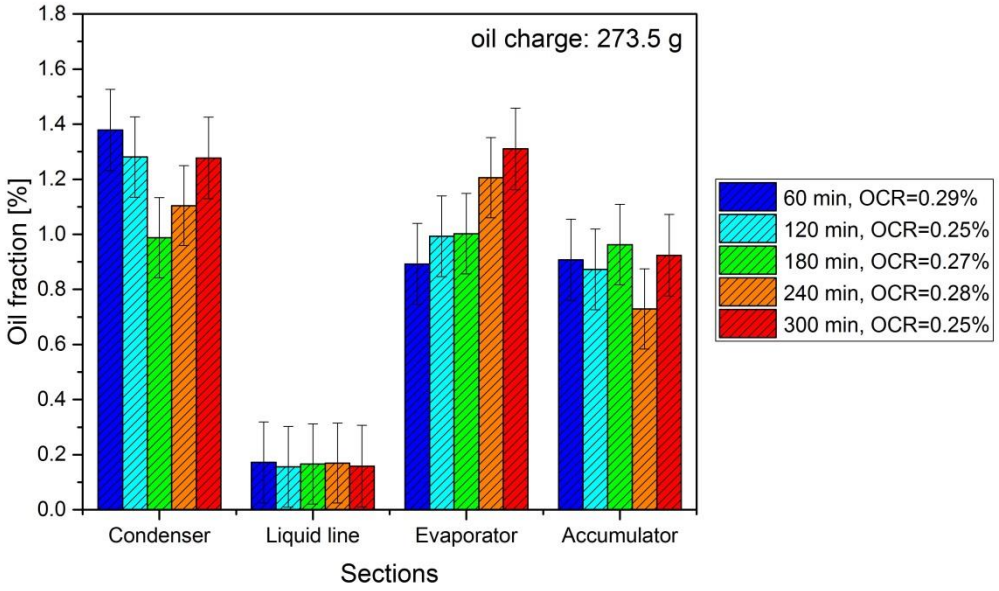

Figure 4.7 Distribution of oil during five hours' heating of the tank

To explain the oil retention change in two heat exchangers, following conceptual analysis could be helpful. To start with, it is important to assume that oil always flows with the liquid refrigerant as the homogeneous refrigerant-oil mixture. Therefore, the velocity of the oil flow is the same as the velocity of the liquid refrigerant. The next assumption in this analysis should be no oil is held up and all oil is flowing with the liquid refrigerant. With these two assumptions, the retained mass of the oil in a section can be estimated by the oil mass flow rate multiplying the time needed for one oil molecule flowing through the entire section:

$$M_{oil} = \dot{m}_{oil} \cdot \Delta t_{oil} = \dot{m}_{oil} \cdot \frac{L_{section}}{\bar{u}_{oil}} = OCR \cdot \dot{m}_{total} \cdot \frac{L_{section}}{\bar{u}_{liq}} \qquad (4.5)$$

Here, $\dot{m}_{\text{total}}$ is the total mass flow rate of refrigerant and oil; $L_{section}$ is the length of the section; $\bar{u}_{oil}$ and $\bar{u}_{liq}$ is average velocity of oil and liquid refrigerant respectively, and they should be equal according to the assumption above. Since in this HPWH system, the OCR and $\dot{m}_{total}$ are relatively unchanged during the heating, the oil retention in a section is mainly determined by the average velocity of the liquid refrigerant (or liquid mixture). The liquid velocity of refrigerant in two-phase region can be expressed as following:

$$u_{liq} = \frac{\dot{m}_{total} \cdot (1 - x_{mix})}{\rho_{liq} \cdot A \cdot (1 - \alpha)} \tag{4.6}$$

Here, A is the cross-sectional area of the tube, and x_{mix} is the vapor quality of the refrigerant-oil mixture. Furthermore, the void fraction can be directly related to the quality by many models. This will be discussed in the next Chapter. By applying the void fraction model and density correlation of the liquid refrigerant-oil mixture, it is found that the liquid velocity is decreasing with an increased quality. The relevant discussion would be in the Chapter 6. Applying this result in the evaporator, with a higher inlet quality, the average liquid velocity in the evaporator should be reduced with the time, and that makes the oil retention increase. In the condenser, during the heating process, the subcooled region and superheat region are both increasing. The ultimate oil retention result indicates that the increase in subcooled region dominates at the beginning, which increases the average liquid velocity, and thus the oil retention decreases. Later, the increase in superheated region takes over, and the average liquid velocity decreases which increases the oil retention. This explanation matches with the fact that the system subcooling increases dramatically in the early stage of the heating, then maintains almost constant.

CHAPTER 5-SYSTEM PERFORMANCE MODELLING

5.1 Model Overview

To simulate the transient system performance of the HPWH during the heating process, a linked EES-CFD system model has been developed. The essence of this model is to simulate the performance of the vapor compression system by a quasi-steady-state mathematical model (built in Engineering Equation Solver, EES [17]) and to model the heat transfer and flow field in the water tank by a CFD model (developed in ANSYS Fluent). These two models are connected at the interface of the tank wall and the water in the storage tank. The CFD model provides temperature and velocity information of the water in tank to the EES model for heat transfer calculation. The EES model outputs the heat flux profiles of the tank wall as boundary conditions in the CFD model. The iteration between the CFD model and EES model is needed to get the matched solutions of these two models. This approach is proposed by Shah and Hrnjak [19]. Since the OCR during the heating process is relatively small (<0.3%), the impact of oil on the system performance is neglected and the thermal properties of pure refrigerant are used here.

5.2 Vapor Compression System Model (EES)

As described above, the EES model is a quasi-steady-state model. The quasi-steady-state assumption is made based on the slow nature of the heating process. Usually, it takes around 5 hours to heat water from 25 ^{o}C to 50 ^{o}C. This vapor compression system model consists of three sub-models to simulate the behavior of two heat exchangers and the compressor. The expansion valve is assumed to be isenthalpic. These three sub-models will be described below respectively.

5.2.1 Compressor model

Referring to Staley et al. [20], the compressor is modeled based on the efficiency equations which relate the isentropic and volumetric efficiencies of the compressor to the compression ratio (ratio of discharge and suction pressures). These efficiencies are calculated by simple curve fits (usually linear) relating them to the compression ratio. According to Staley et al. [20], the linear relationship is approximately valid in a wide range of compression ratio. However, it breaks down at very low compression ratios,

where the nonlinear relations are used. The power and refrigerant mass flow rate through the compressor is then obtained with the isentropic and volumetric efficiencies, using following equations:

$$W_{comp} = \frac{W_s}{\eta_s} \tag{5.1}$$

$$\dot{m}_{ref} = \eta_v \cdot \dot{V}_{disp} \cdot \rho_{suc} \tag{5.2}$$

Here, W_s and η_s are the isentropic work and isentropic efficiency respectively. η_v is volumetric efficiency; $\dot{V}_{disp}$ and ρ_{suc} is the displacement rate and suction density of the compressor respectively.

5.2.2 Heat exchanger models

The heat exchangers are modeled by the finite volume method. To calculate the heat transfer between the refrigerant and other side fluids (air for the evaporator, water for the condenser), the Effectiveness- Number of Transfer Unit (ε-NTU) method is used in both evaporator and condenser. As outlined by Incropera and DeWitt [21], the maximum possible heat transfer in one finite volume is defined as

$$Q_{max} = C_{min} \cdot \left(T_{hot,in} - T_{cold,in}\right) \tag{5.3}$$

Where C_{min} is the smaller heat capacity rate between two fluids. And the heat capacity rate is defined as the product of mass flow rate and the specific heat of the fluid.

The actual heat transfer in one element can be expressed as

$$Q = \varepsilon \cdot C_{min} \cdot \left(T_{hot,in} - T_{cold,in}\right) \tag{5.4}$$

And the effectivenessε, is then defined as the ratio between the actual heat transferred to the maximum possible heat transfer

$$\varepsilon = \frac{Q}{Q_{max}} \tag{5.5}$$

The effectiveness is a function of the NTU and heat capacity ratio C_r, which is defined as the ratio of the smaller heat capacity rate to the larger heat capacity rate of two fluids:

$$C_r = \frac{C_{min}}{C_{max}} = \frac{min(C_{hot}, C_{cold})}{max(C_{hot}, C_{cold})} \tag{5.6}$$

And the number of transfer unit, NTU, is given by the Equation (5.7) below

$$NTU = \frac{UA}{C_{min}} \tag{5.7}$$

The overall heat transfer coefficient UA, is calculated by the thermal resistance between two fluids:

$$\frac{1}{UA} = \frac{1}{h_{hot}A_{hot}} + \frac{\delta_{wall}}{k_{wall}A_{hot/cold}} + \frac{1}{h_{cold}A_{cold}} \tag{5.8}$$

Where h_{hot} and h_{cold} is the heat transfer coefficient in hot and cold fluid side. k_{wall} is the thermal conductivity of the wall evaluated at the average wall temperature. And δ_{wall} is the thickness of the wall.

The flow in two heat exchangers of this HPWH is approximately cross flow. The relation between the effectiveness and the NTU in the single phase cross flow is derived as

$$\varepsilon = 1 - exp\left[\left(\frac{1}{C_r}\right) \cdot NTU^{0.22} \cdot (exp[-C_r \cdot NTU^{0.78}] - 1)\right] \tag{5.9}$$

And in two-phase region, following equation is used

$$\varepsilon = 1 - exp(-NTU) \tag{5.10}$$

By solving the Equation (5.3) ~ (5.10), the heat transfer, as well as the outlet temperature of two fluids for each element can be obtained. The calculation of heat transfer coefficient and the pressure drop in each heat exchanger will be discussed below.

Evaporator

The evaporator used in this HPWH system is a fin-and-tube heat exchanger. Some geometry information of the evaporator is listed in Table 5.1.

Table 5.1 Evaporator geometry

Width [m]	0.432	Tube material	Cu
Height [m]	0.343	Transverse tube spacing [m]	0.024
Circuits	2	Longitudinal tube spacing [m]	0.016
Passes per circuit	13	Fin density [m^{-1}]	630
Inner tube diameter [mm]	7.9	Fin pitch [mm]	1.59
Outer tube diameter [mm]	8.5	Fin thickness [mm]	0.11

For the evaporator, the Equation (5.8) needs to be modified to take the effect of fin into account. A surface efficiency η_f is introduced into the equation:

$$\frac{1}{UA} = \frac{1}{\eta_f h_{air} A_{air}} + \frac{\delta_{wall}}{k_{wall} A_{ref}} + \frac{1}{h_{ref} A_{ref}} \tag{5.11}$$

The air side heat transfer coefficient h_{air} is evaluated using the correlation proposed by Wang et al. [22], in which the non-dimensional Coburn factor is given as

$$j = 0.086 \cdot Re_{D_c}^{P1} \cdot N_r^{P2} \cdot \left(\frac{F_P}{D_c}\right)^{P3} \left(\frac{F_P}{D_h}\right)^{P4} \left(\frac{F_P}{P_t}\right)^{-0.93} \tag{5.12}$$

Where Re_{D_c} is the Reynolds number based on the tube collar diameter, N_r is the number of tube row, F_P is the fin pitch and D_h is the hydraulic diameter of air flow. Four exponents in the Equation (5.12) are calculated by following equations:

$P1 = -0.361 - \frac{0.042 N_r}{ln(Re_{D_c})} + 0.158 ln\left[N_r \left(\frac{F_P}{D_c}\right)^{0.41}\right]$;

$P2 = -1.224 - \frac{0.076\left(\frac{P1}{D_h}\right)^{1.42}}{ln(Re_{D_c})}$;

$P3 = -0.083 + \frac{0.058 N_r}{ln(Re_{D_c})}$;

$P4 = -5.735 + 1.211 \ln\left(\frac{Re_{D_c}}{N_r}\right)$.

Thereby, the air side heat transfer coefficient can be obtained by:

$$h_{air} = G_{air} \cdot c_{p,air} \cdot Pr_{air}^{-0.667} \cdot j \tag{5.13}$$

For the refrigerant side, the single phase heat transfer coefficient is calculated by the Gnielinski's correlation [23]. This correlation is developed for the turbulent flow in a circular tube.

$$Nu_D = \frac{(f/8)(Re_D - 1000) Pr_{ref}}{1 + 12.7(f/8)^{1/2}\left(Pr_{ref}^{2/3} - 1\right)} \tag{5.14}$$

In the Equation (5.14), f is the Darcy friction factor, which can either be obtained from the Moody chart or more precisely using the friction factor correlation discussed later.

And the single phase heat transfer coefficient is given by

$$h_{ref} = \frac{Nu_D \cdot D}{k_{ref}} \tag{5.15}$$

Referring to Wattelet et al. [24], the refrigerant two-phase heat transfer coefficient in the evaporator can be calculated by the asymptotic model:

$$h_{tp} = [h_{nb}^n + h_{cb}^n]^{1/n} \tag{5.16}$$

The Equation (5.16) basically decomposes the total two phase heat transfer coefficient (h_{tp}) into two components: nucleate boiling (h_{nb}) and convective boiling (h_{cb}). In Wattelet et al. [24], the exponent n is recommended to be 2.5. The nucleate and convective boiling components are computed by following correlations:

$$h_{nb} = 55q''^{0.67} {W_m}^{-0.5} Pr_{ref}^{0.12} \left[-log_{10}\left(Pr_{ref}\right)\right]^{-0.55} \tag{5.17}$$

$$h_{cb} = \mathrm{F}h_{liq}R \tag{5.18}$$

$$F = 1 + 1.925X_{tt}^{-0.83} \tag{5.19}$$

$$h_{liq} = 0.023 \frac{k_{ref,liq}}{D} Re_{liq}^{0.8} Pr_{liq}^{0.4} \tag{5.20}$$

$$R = 1.32Fr_{liq}^{0.2} \text{ , for } Fr_{liq} < 0.25 \tag{5.21a}$$

$$R = 1, \text{for } Fr_{liq} \geq 0.25 \tag{5.21b}$$

In above equations, q'' is the heat flux; W_m is the molecular weight of refrigerant; $Re_{liq}$and Pr_{liq} are Reynolds number and Prandtl number using liquid properties; Fr_{liq} is the liquid Froude number, which is defined as:

$$Fr_{liq} = \frac{G_{ref}^2}{\rho_{ref,liq} g D} \tag{5.22}$$

And X_{tt} is the Lockhart-Martinelli number, in the form of

$$X_{tt} = \left(\frac{1-x}{x}\right)^{0.875} \left(\frac{\rho_v}{\rho_l}\right)^{0.5} \left(\frac{\mu_l}{\mu_v}\right)^{0.125} \tag{5.23}$$

To calculate the single phase pressure drop in refrigerant side, Churchill's friction factor correlation [25] has been selected in the model. It is an explicit curve fitting of Moody's friction factor plots in both laminar and turbulent regions with smooth or rough pipes.

$$f_c = \left[\left(\frac{8}{Re}\right)^{12} + \frac{1}{(A+B)^{3/2}}\right]^{1/12} \tag{5.24}$$

Where A $= \left[2.475 \left(\frac{1}{\left(\frac{7}{Re}\right)^{0.9} + 0.27\frac{\varepsilon}{D}}\right)\right]^{16}$, and B $= \left(\frac{37530}{Re}\right)^{16}$, and ε is the surface roughness of the tube.

For the two phase refrigerant flowing through a horizontal tube, the total pressure drop

can be decomposed into two components: frictional pressure drop (ΔP_f) and acceleration pressure drop (ΔP_a), hence:

$$\Delta P_{tp} = \Delta P_f + \Delta P_a \tag{5.25}$$

From the momentum balance, the acceleration pressure drop can be calculated based on the knowledge of void fraction:

$$\Delta P_a = G_{ref}^2 \left\{ \left[\frac{{x_o}^2}{\rho_v \alpha_o} + \frac{(1-x_o)^2}{\rho_l (1-\alpha_o)^2} \right] - \left[\frac{{x_i}^2}{\rho_v \alpha_i} + \frac{(1-x_i)^2}{\rho_l (1-\alpha_i)^2} \right] \right\} \tag{5.26}$$

The subscript *i* and *o* denote the inlet and outlet of the control volume respectively.

To determine the frictional component of the pressure drop for two-phase flow, many two-phase pressure drop correlations take the form of a two-phase multiplier ϕ_x, where the two-phase pressure drop is related to either the liquid or vapor single-phase pressure drop. A semi-empirical correlation proposed by Souza and Pimenta [26] for horizontal tubes, is selected to calculate one of the two-phase multipliers, ϕ_{lo}, which is defined as the ratio of two-phase frictional pressure gradient to the frictional pressure gradient if all refrigerant flows as a liquid:

$$\phi_{lo} = \left(\frac{\partial P}{\partial z}\right)_f \Big/ \left(\frac{\partial P}{\partial z}\right)_{lo} \tag{5.27}$$

The selected correlation is in forms of:

$${\phi_{lo}}^2 = 1 + (\Gamma^2 - 1) x^{1.75} \left(1 + 0.9524 \Gamma X_{tt}^{0.4126}\right) \tag{5.28}$$

Where $\Gamma = \left(\frac{\rho_l}{\rho_v}\right)^{0.5} \left(\frac{\mu_v}{\mu_l}\right)^{0.125}$, is the physical property index.

The frictional gradient of total liquid flow is then calculated by:

$$\left(\frac{\partial P}{\partial z}\right)_{lo} = \frac{f_{lo} G_{ref}^2}{2 \rho_l D} \tag{5.29}$$

f_{lo} is the single phase (liquid) Darcy friction factor, which can be calculated through the Equation (5.24).

The calculation of two phase pressure drop is on the basis of estimation of the void fraction (see Equation (5.26)). In a vapor-liquid two phase flow, the void fraction is usually defined as the fraction of the cross-sectional area occupied by the gas phase with respect to the total cross-sectional area of the flow. In this model, the void fraction is

predicted by the correlation proposed by Rouhani and Axelsson [27], which is in forms of:

$$\alpha = \frac{x}{\rho_v}\left\{C\left[\frac{x}{\rho_v}+\frac{1-x}{\rho_l}\right]+\frac{1.18}{G_{ref}}\left[\frac{\sigma_{ref}\,g(\rho_l-\rho_v)}{{\rho_l}^2}\right]^{0.25}\right\}^{-1} \tag{5.30}$$

Where $C = 1 + 0.2(1-x)$, and σ_{ref} is the surface tension of the refrigerant.

Condenser

The condenser in this HPWH system has two parallel circuits of tube coils wrapped around the wall of the water tank. Each parallel circuit has 13 coils and the superheated refrigerant is configured to enter the topmost coil and leave subcooled through the bottommost coil. For the convenience of modeling, it is assumed no maldistribution of the refrigerant between these two circuits and the local states of the refrigerant in two circuits are identical. This means, these two parallel circuits can be simplified as one circuit with a doubled cross-sectional area and a doubled contact area with the wall. But the hydraulic diameter is maintained as its original value in the calculation of heat transfer and pressure drop. Appling finite volume method, the condenser is defined to have N coils, and each coil is discretized into M elements as shown in Figure 5.1

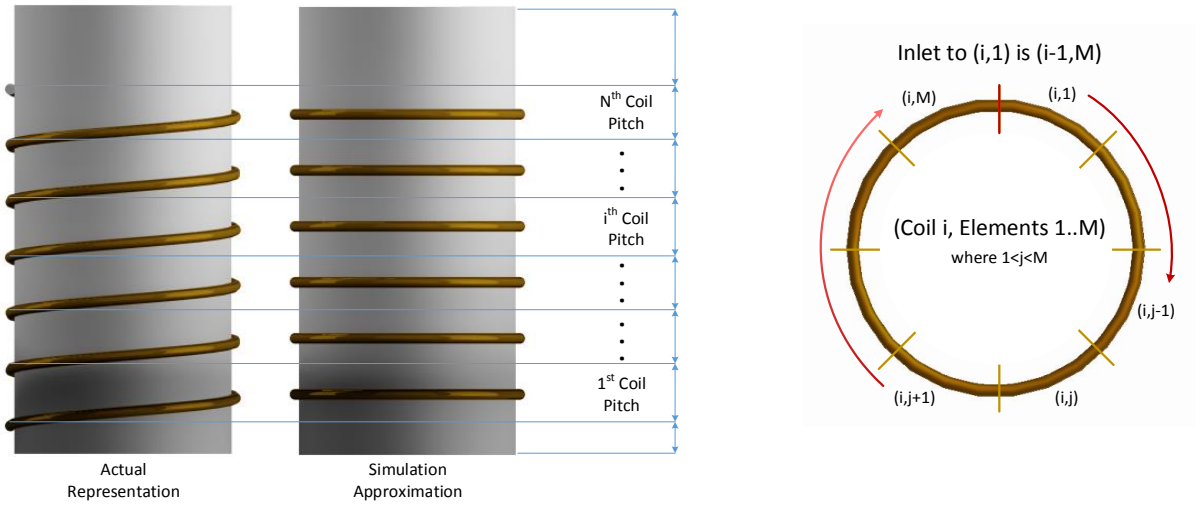

Figure 5.1 Adaptation of coils windings and discretization of each coil into element, adapted from [19]

The simulation of each coil element is shown in Figure 5.2. Each coil element has a corresponding segment of the tank wall and an upward flow water stream which is in a cross flow arrangement with the refrigerant flow. This three-part arrangement thus composes a series of thermal resistance from refrigerant to water. The height of the tank

wall in each element is determined by the coil pitch as shown in Figure 5.1. Furthermore, the refrigerant coils and the water tank walls can be simplified to be fins in external flow as shown in Figure 5.3. The value for the contact resistance is generally estimated with available data.

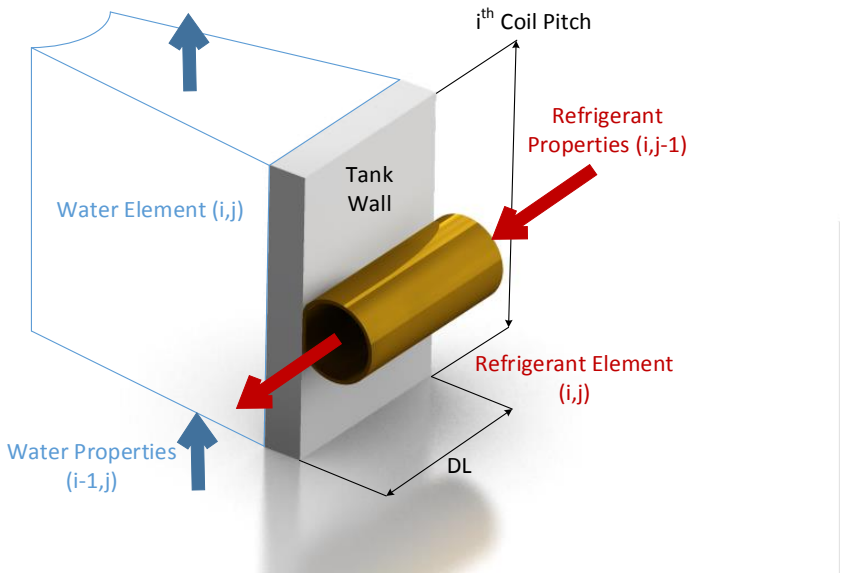

Figure 5.2 Single element of condenser, adapted from [19]

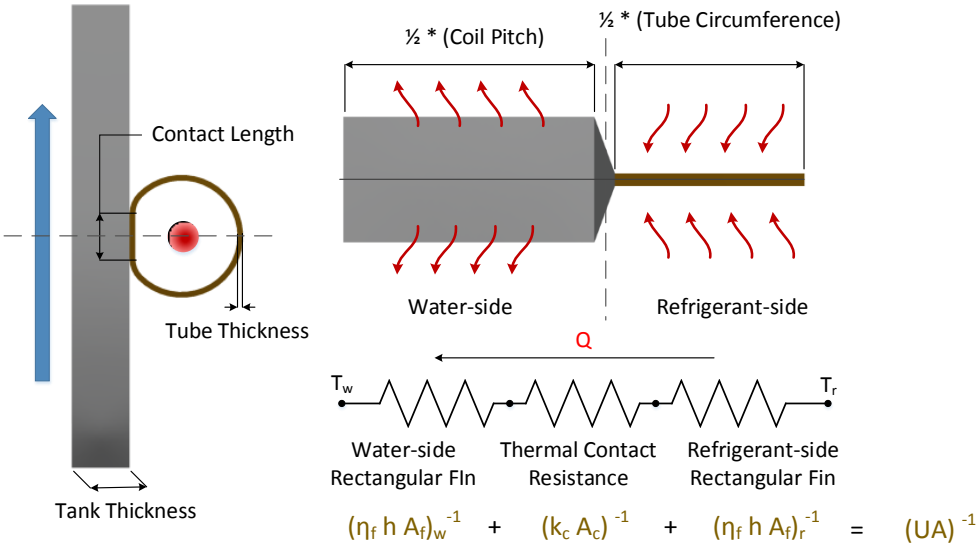

Figure 5.3 Element simplification and description of heat path, adapted from [19]

To evaluate the heat transfer coefficients and pressure drop in the condenser, the same correlations used in the evaporator calculation are employed again, except for the two phase heat transfer correlations. The condensing heat transfer coefficient is estimated

using Dobson and Chato's correlations [28]. In Dobson and Chato's work, the heat transfer coefficient was directly connected to the different flow regimes during the condensation. Stratified, wavy, wavy annular, annular, annular mist, and slug flows were observed in their experiments for smooth horizontal tubes. Heat transfer correlations were developed for each of these flow regimes. Therefore, the calculation of the heat transfer coefficient requires the prediction of flow regime, which is also given in Dobson and Chato's paper [28]. Due to the complexity of the equations, it is not elaborately discussed here.

As described above, the water near the tank wall is directly heated by the wall and flows upward due to the buoyancy. A thin upward flow layer is then defined, in which water has an upward velocity component. The water outside of the upward flow layer generally has a downward velocity component because of the water circulation in the tank. The thickness of the upward flow layer is set to be 1 cm based on the CFD simulation, which will be discussed later. This thickness is also used for averaging the temperature and velocity of the upward water flow. The heat transfer correlation for the laminar external flow over a flat plate is then used to calculate the water side heat transfer coefficient:

$$Nu = 0.664 Re^{1/2} Pr^{1/3} \tag{5.31}$$

In the Equation (5.31), the characteristic length is chosen to be the thickness of the upward flow layer.

5.3 Water Tank CFD Model

A CFD model is established in ANSYS Fluent to simulate the temperature and flow fields in the water tank during the heating process. Considering the symmetry in the water tank geometry and physical boundary conditions, this CFD model is designed to be a two-dimensional (2-D) axisymmetric domain, shown in Figure 5.4. The axisymmetric boundary corresponds to the centerline of the cylindrical water tank. Structured quadrangular mesh is used in this simulation. To better capture the thermal and momentum interactions between the water and tank wall, boundary layer grids have been used to intense the grid density near the wall. The mesh contains 20280 cells in total. In this CFD model, each condenser coil is accounted by a line segment of the side wall

boundary. The length of each segment is the corresponding coil pitch. The model then assumes that for each segment, heat flux is uniform on the surface of the segment. The User Defined Function (UDF) file is then used to specify the temporal heat flux profiles for each coil, which can be obtained from the quasi-steady-state modeling of the vapor compression system.

The simulation is conducted under unsteady setting to cover a full 5 hours' heating. The time step is selected to be 3 s. SIMPLEC scheme is selected for pressure-velocity coupling. The density variation induced by the temperature change is accounted through the Boussinesq approximation. This approximation treats density as a constant value in all solved equations, except for the buoyancy term in the momentum equation. In addition, it assumes the density changes linearly with the temperature. The buoyancy driven flow is assumed to be laminar.

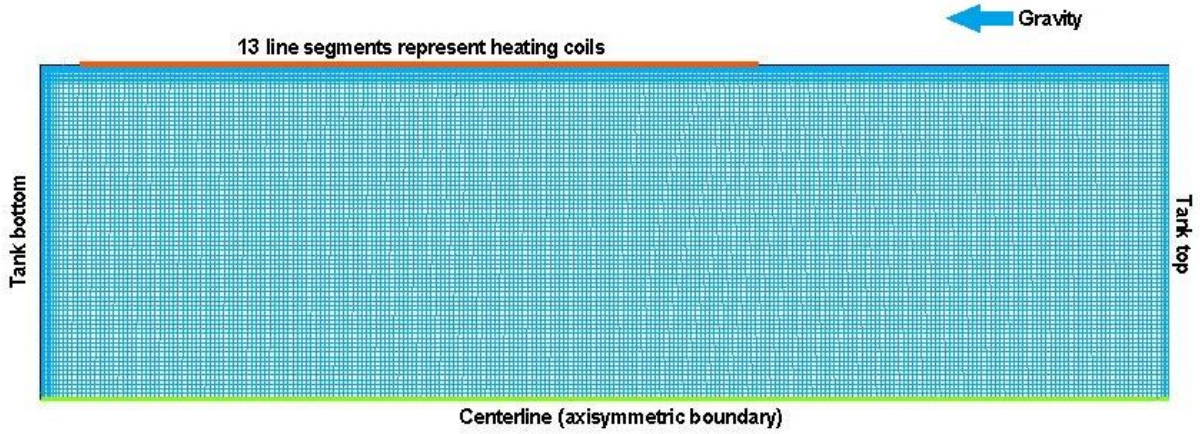

Figure 5.4 Geometry and mesh of the water tank CFD model

The key output of the CFD modeling is the average temperature and velocity of water in the vicinity of each coil at various points of time, which would be utilized in the system model (EES) for the calculation of water side heat transfer.

5.4 Linked Algorithm between the EES Model and CFD Model

As mentioned above, the system model (EES) and water tank model (CFD) are connected by the information exchange through the tank wall. The CFD model provides near-wall water temperature and velocity information to the EES model for heat transfer calculation. The EES model outputs a heat flux profile of coils as boundary conditions in the CFD simulation. To get the matched solutions of these two models, the iteration between the

CFD and EES model is needed.

The flowchart in Figure 5.5 shows the linked algorithm used in the calculation. Basically, the iteration is initiated with a guessed coil heat flux profile. With this profile, the CFD model runs the first simulation for a full heating process. Then the near-wall water temperature and velocity profiles obtained from CFD modeling is utilized in the EES model to update a new heat flux profile for the next CFD running. The alternate running of the CFD and EES model, as well as the information exchange between them will be continued until the heat flux profile stabilizes (variation between iterations <1%).

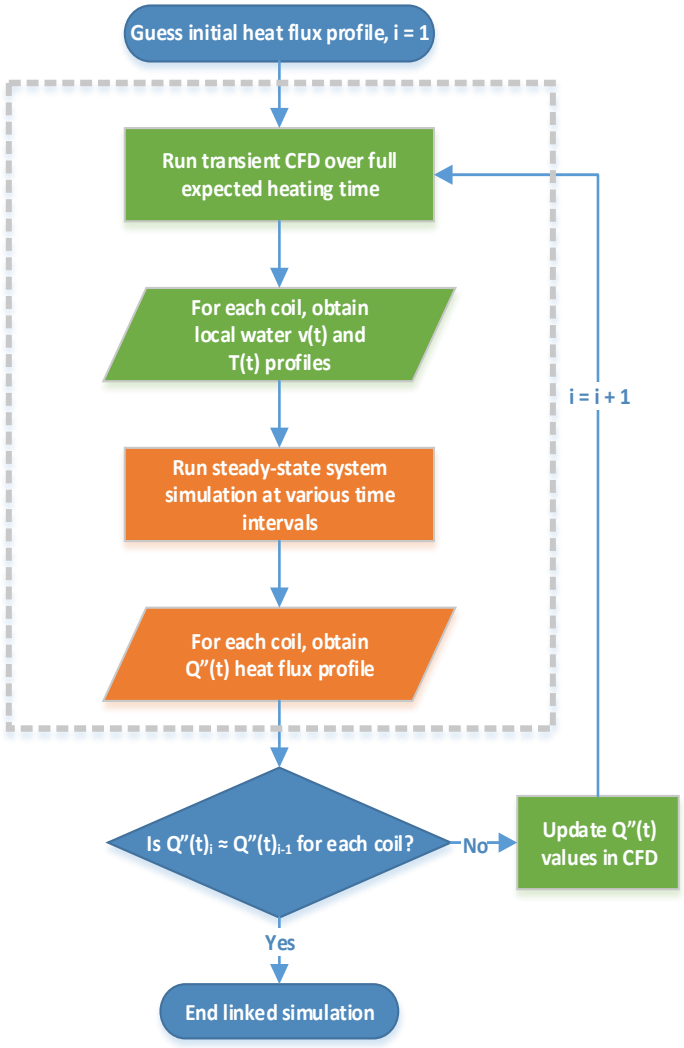

Figure 5.5 Linked algorithm between the EES and CFD model, adapted from [19]

5.5 Results and Discussion

Figure 5.6 presents the comparison between the experimental data and model prediction for the capacities of two heat exchangers, the compressor work and COP of the system. It

can be concluded from the Figure 5.6 that the linked EES-CFD model gives a good agreement with the experimental data. The model quantitatively captures the transient changes of the capacities of two heat exchangers and the compressor work with the time. It also gives a fairly good prediction of the system COP. The average deviation between the measurement and the prediction of the capacities and power is 4.2%. While, the deviation in COP prediction is 2.0%. But observing the deviation between the experimental results and the model prediction, one could find the predictions are more accurate for points earlier in the time.

As described before, three series of thermocouples are placed in the water tank to monitor the water temperature change. The average temperature of these three thermocouple series at different time points can also be predicted by CFD modeling. In the prediction, the centerline in the computational domain is used to represent the vertical thermocouple series; two horizontal thermocouple series are predicted by two lines at the corresponding heights. The comparison between the measured and predicted average water temperature is shown in Figure 5.7.

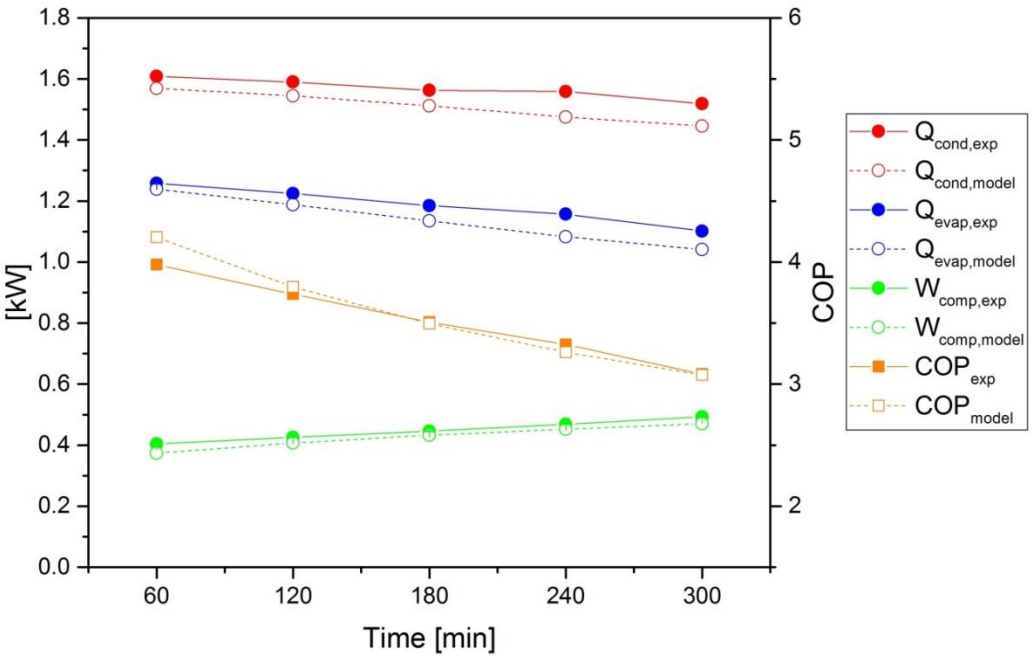

Figure 5.6 Experiments vs. modeling: capacities, power and COP

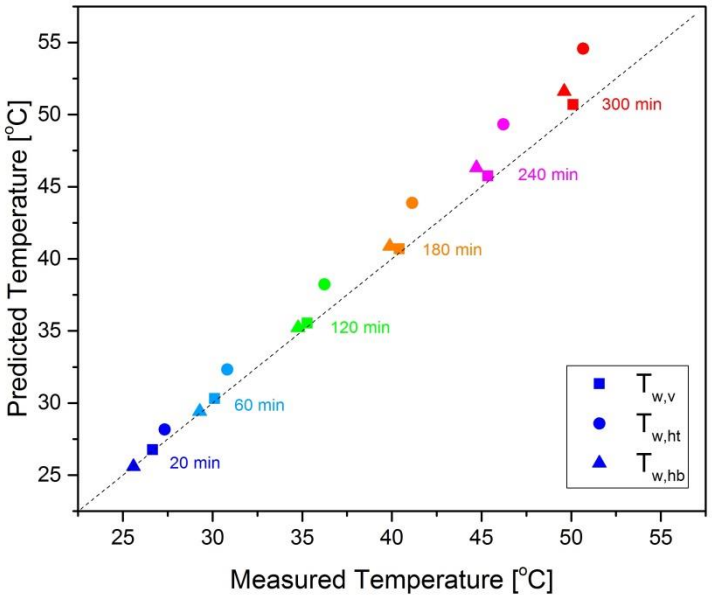

Figure 5.7 Experiments vs. modeling: average water temperature

It can be clearly seen in Figure 5.7 that the predicted average temperature of the vertical thermocouple series matches the experimental data fairly well. However, the CFD model seems to overestimate the average temperature of two horizontal thermocouple series and the deviations are enlarged with the time. This is similar to the prediction of capacities in Figure 5.6. One possible reason for this increased deviation is, the Boussinesq approximation used in CFD modeling is only applicable for a small temperature difference. As the time increased, the intensive stratification of water temperature makes the Boussinesq approximation deviate from the reality.

Nevertheless, the CFD model is still a very good tool to visualize the flow and temperature fields in the water tank during the heating process. Figure 5.8 and 5.9 give the velocity trajectories and temperature contours of the water tank at t=60 min and t=300 min respectively.

It can be clearly observed that the upward flow water is confined in a thin layer near the tank wall. Water outside of this thin layer is mainly flowing downward. This is thin layer is defined to be the upward flow layer as mentioned before. The thickness of this layer is selected to be 1 cm based on the simulation results. Comparing Figure 5.8 (a) and Figure 5.9 (a), it seems that the flow patterns at these two time points are quiet similar. They only differ a little bit in velocity magnitude. However, when it comes to the temperature contours, a significant difference can be found at these two time points. Obviously, the

stratification of the water temperature is more intensive for a longer heating time. The temperature difference between the top and bottom layer of water reaches about 25 ^{o}C after system running for 5 hours. The Boussinesq approximation may break down at such a high temperature difference.

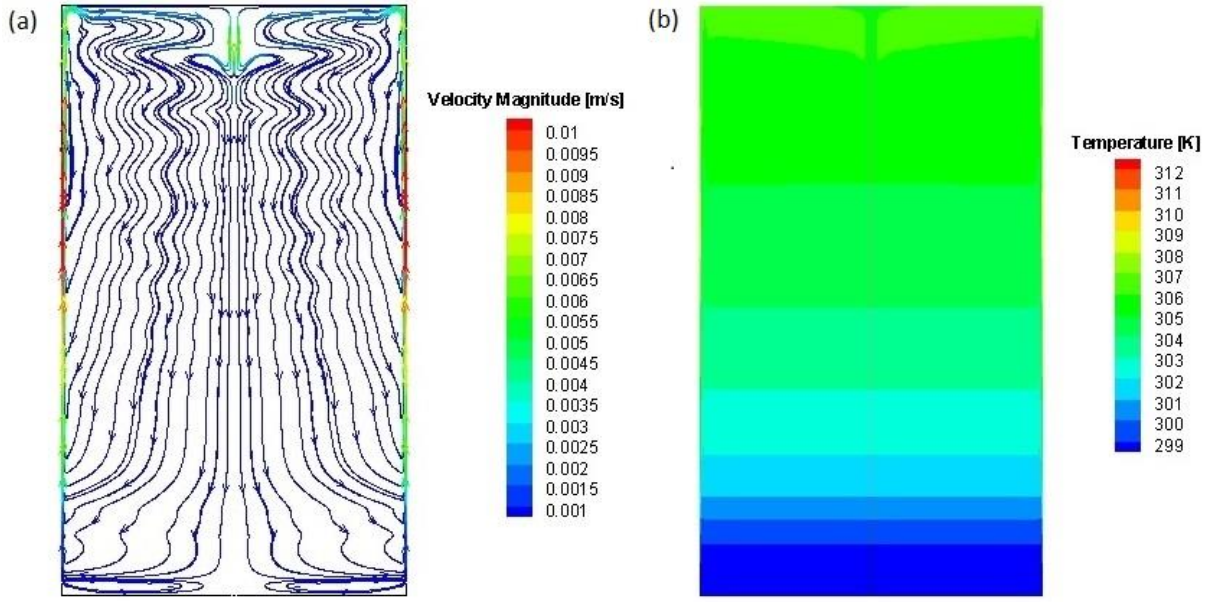

Figure 5.8 Velocity trajectories (a) and temperature contours (b) of the water tank at t=60 min

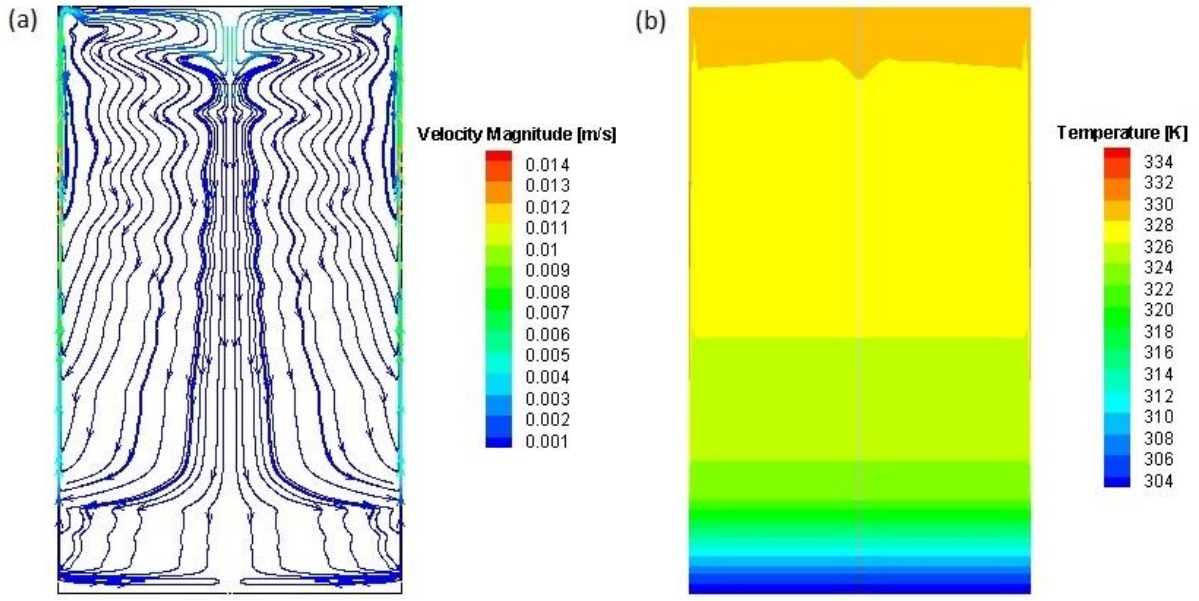

Figure 5.9 Velocity trajectories (a) and temperature contours (b) of water tank at t=300 min

CHAPTER 6-MODEL OF REFRIGERANT AND OIL RETENTION IN HEAT EXCHANGERS

In Chapter 5, a linked EES-CFD model is developed to simulate the system performance during the heating process of the HWPH unit. In that model, the effect of oil is neglected due to a relatively small system OCR. In this Chapter, a model to predict the refrigerant and oil retention in the heat exchangers has been established on the basis of previous system modeling results.

6.1 Oil-Refrigerant Mixture Properties

To predict the refrigerant and oil retention in the heat exchangers, the thermoproperties of the refrigerant-oil mixture are employed. Since it is assumed that all oil is circulating with the liquid refrigerant and forms a homogenous mixture of liquid phase, the impact of oil is only limited in the liquid phase. This retention model involves three thermal properties of the mixture: solubility, density and surface tension.

To estimate the solubility between R134a and POE 22 oil, Henderson [29] curve fitted the experimental data and proposed two empirical correlations depending on the refrigerant concentration in the mixture. For a low refrigerant concentration mixture, the correlation is in forms of:

$$P = (a_1 + a_2 T + a_3 T^2) + \omega(a_4 + a_5 T + a_6 T^2) + \omega^2(a_7 + a_8 T + a_9 T^2) \quad (6.1)$$

Where P is the vapor pressure in kPa, T is the temperature in K, and ω is the mass fraction of refrigerant in mixture. $a_1 \sim a_9$ are constants whose values are summarized in Table 6.1. Equation (6.1) is claimed to be applicable for ω smaller than 30%.

The solubility correlation for a high refrigerant concentration (ω >80%) is given in Equation (6.2):

$$log_{10}(P) = (a_1' + a_2'/T + a_3'/T^2) + \omega(a_4' + a_5'/T + a_6'/T^2) + \omega^2(a_7' + a_8'/T + a_9'/T^2) \quad (6.2)$$

The values of $a_1' \sim a_9'$ are also given in Table 6.1.

Henderson [29] also proposed two correlations for the density of R134a and POE 22 mixture in the same manner. For a low refrigerant concentration (ω <30%):

$$\rho_{mix} = (b_1 + b_2 T + b_3 T^2) + \omega(b_4 + b_5 T + b_6 T^2) + \omega^2(b_7 + b_8 T + b_9 T^2) \quad (6.3)$$

And for a high refrigerant concentration (ω >80%):

$$\rho_{mix} = \left(b_1' + b_2' T_r + b_3' T_r^2\right) + \omega\left(b_4' + b_5' T_r + b_6' T_r^2\right) + \omega^2\left(b_7' + b_8' T_r + b_9' T_r^2\right) \quad (6.4)$$

In Equation (6.3) and (6.4), the density is in g/cc. $T_r = 1 - \frac{T}{T_c}$, T_c is the critical temperature of the refrigerant. Constants $b_1 \sim b_9$ and $b_1' \sim b_9'$ are listed in Table 6.1. The average value of Equation (6.3) and (6.4) is used to fill the gap of ω =30%~70%.

Table 6.1 Constants in Equation (6.1) ~ (6.4)

a_1	2.89782×10^{3}	a_1'	1.53232×10^{1}	b_1	1.13723	b_1'	5.08957×10^{-1}
a_2	-1.80787×10^{1}	a_2'	-2.33421×10^{3}	b_2	-2.89916×10^{-4}	b_2'	-1.82916
a_3	2.79895×10^{-2}	a_3'	-3.89417×10^{5}	b	-6.99544×10^{-7}	b_3'	4.24439
a_4	-1.93339×10^{4}	a_4'	-1.92482×10^{1}	b_4	1.29823	b_4'	1.92860×10^{-1}
a_5	3.73956×10^{1}	a_5'	2.49136×10^{3}	b_5	-5.99345×10^{-3}	b_5'	2.30237
a_6	1.22336×10^{-1}	a_6'	8.95875×10^{5}	b_6	8.03992×10^{-6}	b_6'	-7.28064
a_7	1.97368×10^{5}	a_7'	1.20861×10^{1}	b_7	-1.75900	b_7'	1.99842×10^{-1}
a_8	-1.15833×10^{3}	a_8'	-2.08984×10^{3}	b_8	1.17233×10^{-2}	b_8'	1.05660
a_9	1.62636	a_9'	-4.05323×10^{5}	b_9	-1.95375×10^{-5}	b_9'	2.51343

The liquid mixture surface tension is calculated by the correlation in Jensen and Jackman [30]:

$$\sigma_{mix} = \sigma_{ref} + \left(\sigma_{oil} - \sigma_{ref}\right)\sqrt{c_{oil}} \quad (6.5)$$

Here, c_{oil} is the oil concentration (or oil mass fraction) in the liquid mixture. And Seeton [31] indicated in his thesis that the surface tension of oil can be approximately estimated by:

$$\sigma_{oil} = (35 - 0.15T)/1000 \quad (6.6)$$

In Equation (6.6), σ_{oil} is in N/m, and T is in ^{o}C.

6.2 Model of Refrigerant and Oil Retention in Heat Exchangers

One important assumption in the modeling is that all oil is circulating throughout the

system with liquid refrigerant as a homogenous liquid mixture. In another word, no local oil holdup in the heat exchangers during the system running.

As mentioned above, this retention model is based on the results of the system modeling. In the system model, for each element in the heat exchanger, following information can be obtained: refrigerant mass flow rate ($\dot{m}_{ref}$), refrigerant mass flux (G_{ref}), average quality (x_{ref}), average refrigerant pressure (P_{ref}) and average refrigerant temperature (T_{ref}). Here, the "average" quantity is calculated by averaging the value at the inlet and outlet of an element. For the convenience of modeling, all elements in the heat exchanger can be classified into three categories based on their average quality: superheated, two-phase and subcooled element. Each category will be discussed.

Superheated Element

Superheated elements refer to the elements which have an average quality greater than one. Ideally, there will be no liquid presents in such an element. The entire element should be fully occupied by superheated vapor refrigerant. However, if the oil is taken into account, the situation would be different since the liquid refrigerant-oil mixture will always exist in the element. If the system OCR is known from the experimental data, the mass flow rate of oil can be calculated by:

$$\dot{m}_{oil} = \frac{\dot{m}_{ref} \cdot OCR}{(1 - OCR)} \tag{6.7}$$

Then the solubility between R134a and POE 22 oil is utilized to get the concentration of liquid refrigerant in the mixture. Putting the average pressure (P_{ref}) and average temperature (T_{ref}) into the solubility correlation (Equation (6.1) or (6.2)), the concentration of liquid refrigerant, ω, can be solved out. Thereby, the concentration of oil in mixture is also known:

$$c_{oil} = 1 - \omega \tag{6.8}$$

And the mass flow rate of liquid and vapor refrigerant in the element can be calculated by following two equations:

$$\dot{m}_{ref,liq} = \frac{\dot{m}_{oil} \cdot (1 - c_{oil})}{c_{oil}} \tag{6.9}$$

$$\dot{m}_{ref,vap} = \dot{m}_{ref} - \dot{m}_{ref,vap} \tag{6.10}$$

By knowing $\dot{m}_{ref,vap}$, $\dot{m}_{ref,liq}$ and $\dot{m}_{oil}$, a vapor quality of mixture is defined as:

$$x_{mix} = \frac{\dot{m}_{ref,vap}}{\dot{m}_{ref,liq} + \dot{m}_{ref,vap} + \dot{m}_{oil}} \tag{6.11}$$

Then, the Rouhani and Axelsson's [27] correlation (Equation (5.30)) could be used to calculate the void fraction of the element. The function relationship can be simply expressed as:

$$\alpha = f\left(x_{mix}, \rho_{ref,vap}, \rho_{mix}, G_{ref}, \sigma_{mix}\right) \tag{6.12}$$

Here, ρ_{mix} and σ_{mix} are calculated by the methods discussed above.

Now, the inventory of vapor/liquid refrigerant and oil in the element can be obtained respectively by:

$$M_{ref,vap} = \text{Vol} \cdot \alpha \cdot \rho_{ref,vap} \tag{6.13}$$

$$M_{oil} = \text{Vol} \cdot (1-\alpha) \cdot \rho_{mix} \cdot c_{oil} \tag{6.14}$$

$$M_{ref,liq} = \text{Vol} \cdot (1-\alpha) \cdot \rho_{mix} \cdot (1-c_{oil}) \tag{6.15}$$

Vol in above equations is the internal volume of the element.

Thus, the total retention of refrigerant (M_{ref}) is the summation of $M_{ref,vap}$ and $M_{ref,liq}$.

Two-phase Element

The average quality (x_{ref}) in a two-phase element is between 0 and 1. Both vapor and liquid refrigerant presents in such an element. The mass flow rate of each phase can be calculated through the average quality:

$$\dot{m}_{ref,vap} = \dot{m}_{ref} \cdot x_{ref} \tag{6.16}$$

$$\dot{m}_{ref,liq} = \dot{m}_{ref} \cdot \left(1 - x_{ref}\right) \tag{6.17}$$

The oil mass flow rate ($\dot{m}_{oil}$) can also be obtained by Equation (6.7). Applying the Equation (6.11) ~ (6.15) again, the refrigerant and oil retention in a two-phase element can be obtained.

Subcooled Element

A subcooled element is fully filled with liquid refrigerant-oil mixture. In such an element, the oil concentration should be equal to the system OCR:

$$c_{oil} = OCR \tag{6.18}$$

Therefore, the refrigerant and oil retention can be directly calculated by:

$$M_{oil} = \text{Vol} \cdot \rho_{mix} \cdot c_{oil} \tag{6.19}$$

$$M_{ref} = M_{ref,liq} = \text{Vol} \cdot \rho_{mix} \cdot (1 - c_{oil}) \tag{6.20}$$

The retained mass of the refrigerant and oil in each element is obtained by above procedures. The summation of all elements will be the total retention in the heat exchanger.

6.3 Results and Discussion

Figure 6.1 and 6.2 give comparison between the measured and predicted retention of the refrigerant and oil in the heat exchangers respectively.

Figure 6.1 shows that, the model generally underestimates the refrigerant in both condenser and evaporator. The average deviation between the experimental data and modeling results is 9.9% for the condenser, 15.2% for the evaporator. However, this model successfully captures the transient change of the refrigerant retention in the heat exchangers. It is predicted to have an increased refrigerant retention in the condenser, and a decreased retention in the evaporator.

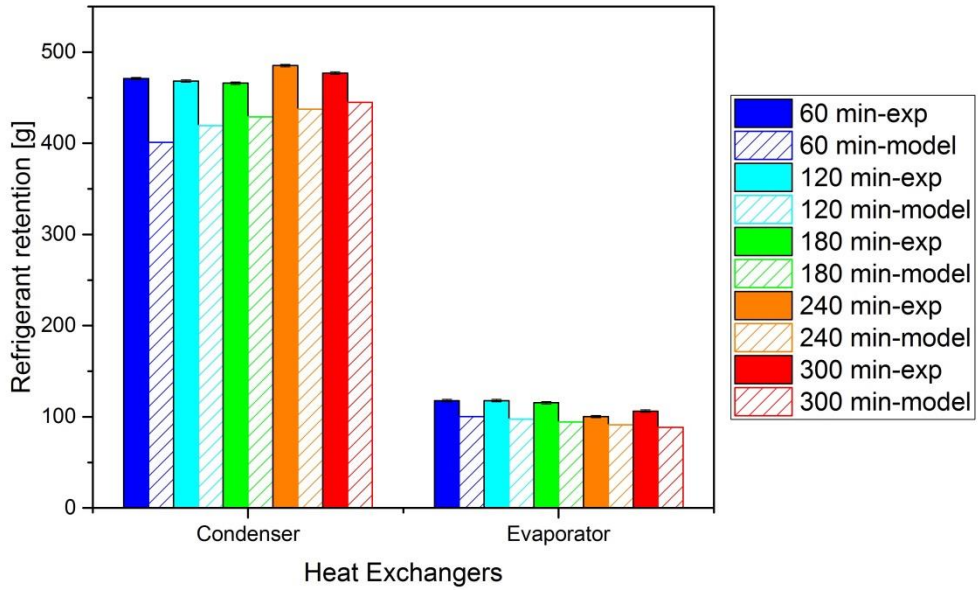

Figure 6.1 Experiments vs. modeling: refrigerant retention in heat exchangers

The deviation in the prediction of oil retention is much larger. The average difference between measured data and modeling results for the condenser and evaporator is 57.5% and 51.6% respectively. It can be seen in the Figure 6.2, that the oil retention in the condenser is overestimated, but in the evaporator, it is underestimated. The model

predicts an increasing retained oil mass in the condenser. But it is measured to decrease first then increase. In the evaporator, a small increase in the oil retention with the time is predicted, which matches with the experimental data.

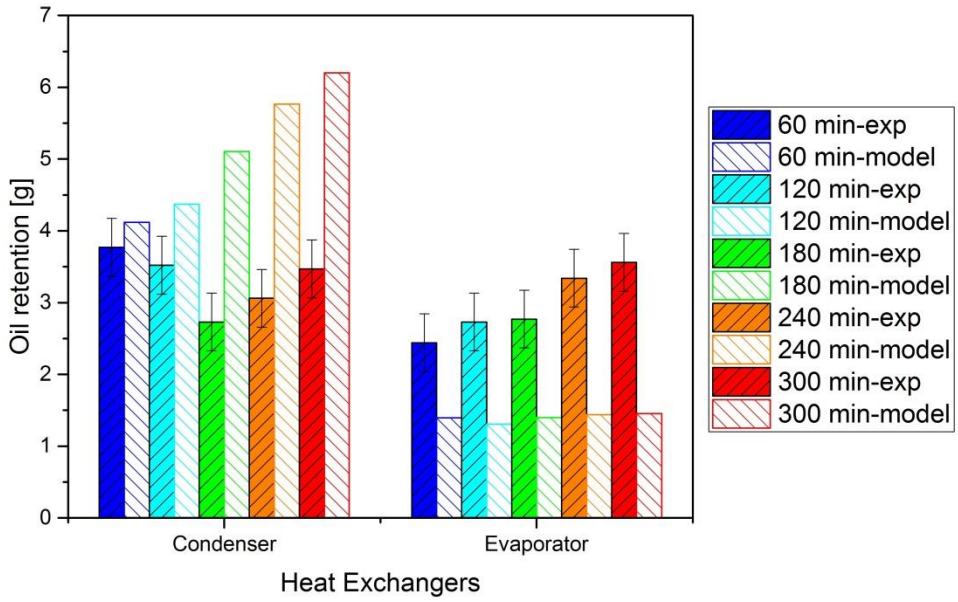

Figure 6.2 Experiments vs. modeling: oil retention in heat exchangers

One merit of this model is capable to provide detailed information about some variables' change in the heat exchangers. Take the case of t=60 min as an example, the changes of oil concentration (c_{oil}), liquid fraction ($1-\alpha$) and vapor quality of the mixture (x_{mix}) throughout the condenser and evaporator are given in Figure 6.3 and 6.4. In the Figure 6.3 and 6.4, the total length of the heat exchanger has been normalized, and the non-dimensional length of 0 and 1 refer to the inlet and outlet of the heat exchanger respectively. The curves of the element oil retention ($M_{\mathrm{oil,e}}$) divided by the non-dimensional element length ($L_{\mathrm{e}}/L_{\mathrm{HX}}$) are also plotted. This curve directly indicates the local distribution of oil in the heat exchangers.

Three different regions can be clearly seen in Figure 6.3: superheated region ($x_{mix} \approx 1$), two-phase region ($1 > x_{mix} > 0$) and subcooled region ($x_{mix} = 0$). In the superheated region, the oil concentration is calculated by the solubility data and keeps nearly constant. When the vapor refrigerant start to condense, the oil is diluted by the liquid refrigerant and the concentration dramatically drops. At the same time, the accumulation of liquid mixture in the tubes makes the liquid fraction increase in the condenser. It is noticeable that the liquid fraction increases even before the

condensation start. This is because the decreasing temperature in the superheated vapor makes it occupy a less volume. Based on the Equation (6.14), the retention oil is approximately proportional to the product of oil concentration and liquid fraction. Therefore, high local oil retention near the inlet of the condenser can be attributed to a high oil concentration at this region; another high retention region of the oil near the outlet is caused by the high liquid fraction.

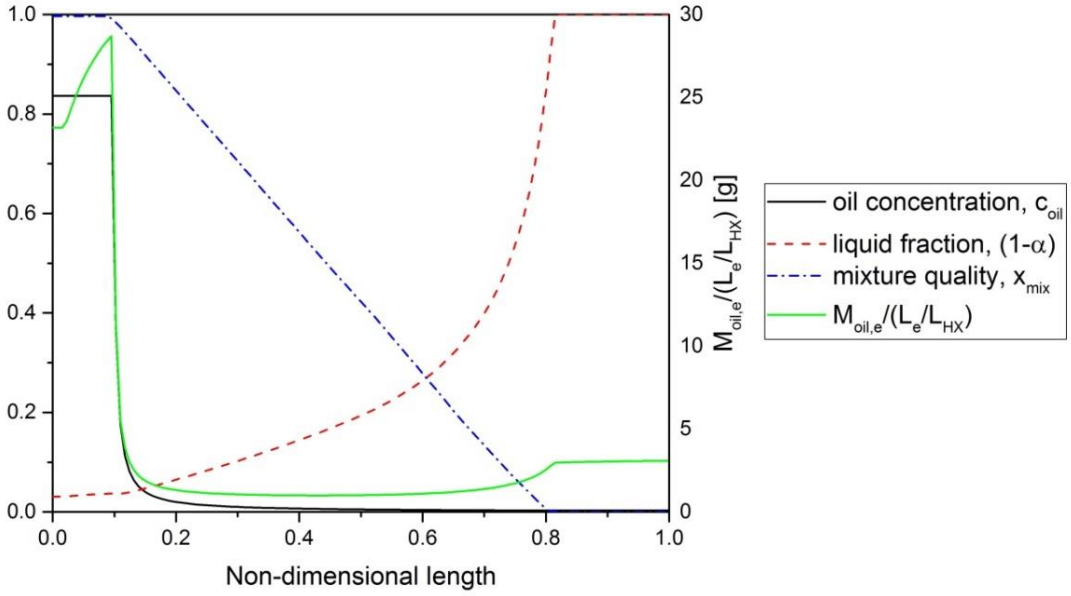

Figure 6.3 Some variables' change in the condenser at t=60 min

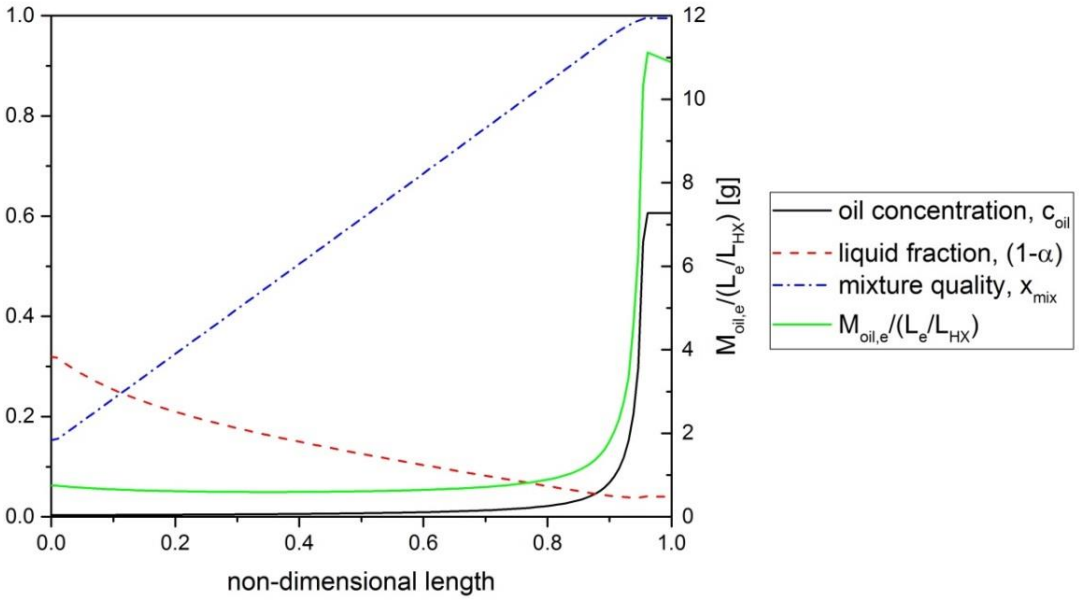

Figure 6.4 Some variables' change in the evaporator at t=60 min

The similar analysis can be used in the evaporator. There is a high oil retention in the vicinity of the evaporator outlet due to a high oil concentration in this region. For

other part of the evaporator, the oil retention is low and quite uniform. This is because a relatively small oil concentration and a moderate liquid fraction in the two-phase region.

To analyze the transient oil retention in the condenser, the curves of oil concentration (c_{oil}), liquid fraction (1-α) and the local distribution of oil at different time points, are shown in Figure 6.5 (a) ~ (c).

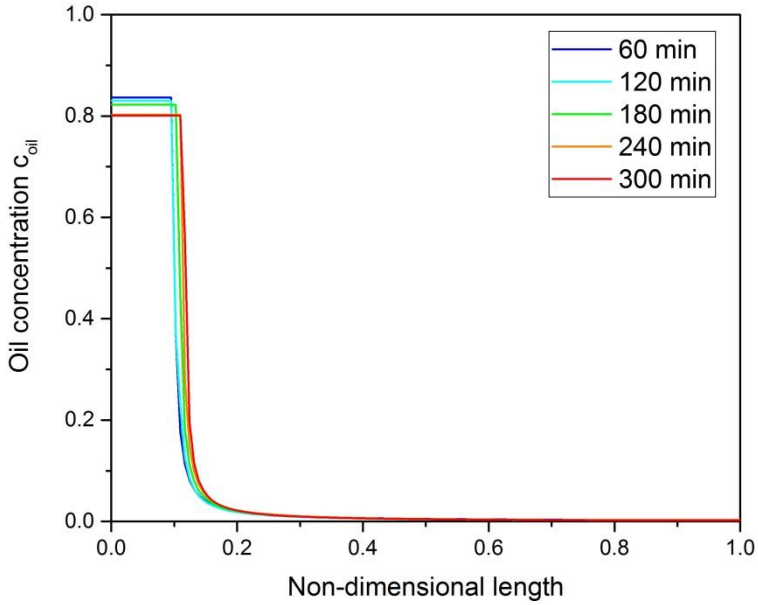

Figure 6.5 (a) Oil concentration curves in the condenser

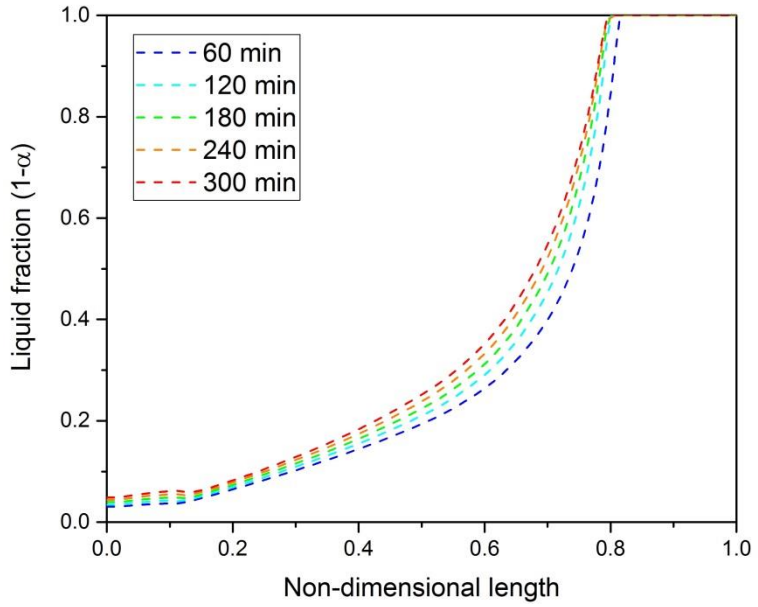

Figure 6.5 (b) Liquid fraction curves in the condenser

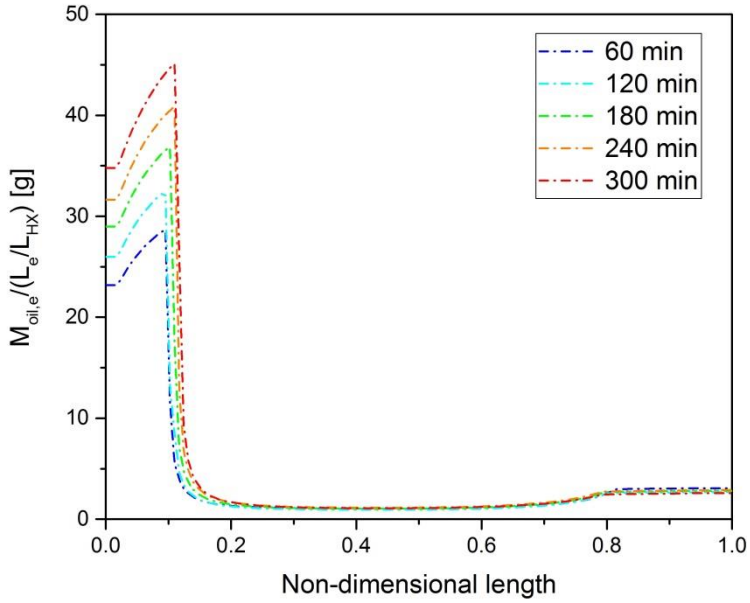

Figure 6.5 (c) Local distribution of oil in the condenser

Firstly, it can be observed in Figure 6.5 (c), that the major oil retention is located at the superheated region. Meanwhile, the difference of oil retention at various time points is also coming from the local oil retention difference in this region. According to the Equation (6.4), the oil retention in the superheated region is determined by the product of liquid mixture density, liquid fraction and oil concentration. Even though, the liquid mixture density and oil concentration decrease with time, but the product is dominated by the liquid fraction, which increases with the time. The data shows an over 60% increase in the liquid fraction at t=300 min compared with t=60 min. That also means the accuracy of the void fraction correlation plays a key role in the prediction of oil retention. This may explain the deviation between the experimental data and modeling results. The modification of this model could focus on selecting a better void fraction model. For example, Xiao and Hrnjak [32] proposed a new void fraction model based on the visualization of flow regime to cover the condensation from the superheated region.

Similar analysis can be applied on the evaporator. Figure 6.6 (a) ~ (c) shows the change of oil concentration (c_{oil}), liquid fraction (1-α) and the local oil distribution in the evaporator. Compared with the situation in the condenser, the difference among the oil retention at various time points is much smaller in the evaporator. The observable difference is mainly located at the regions near the inlet and outlet of the

evaporator. Due to a higher inlet quality, the liquid fraction near the inlet of the evaporator is decreasing with the time, which reduces the oil retention in this region. At the vicinity of the outlet, increased local oil retention mainly comes from a longer superheated region and a higher liquid fraction in this region. The ultimate results indicate that the increase of local oil retention in the superheated region may dominate the change of total oil retention in the evaporator.

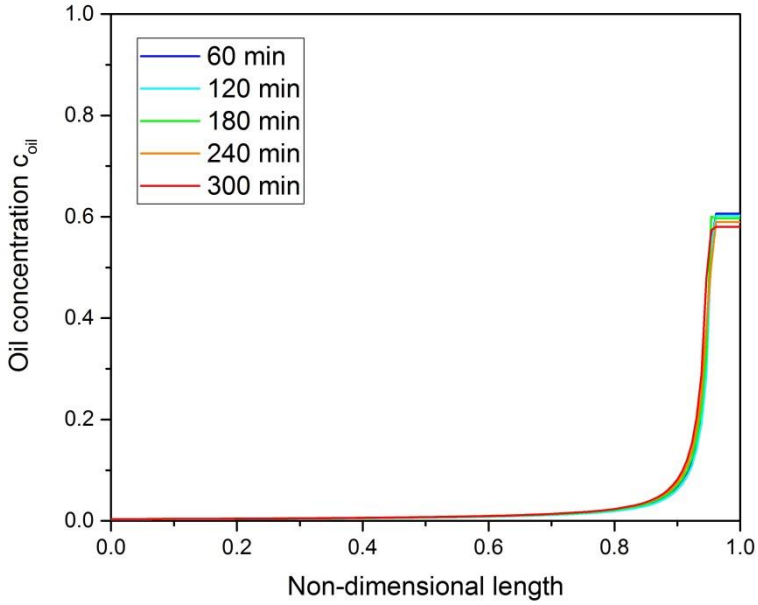

Figure 6.6 (a) Oil concentration curves in the evaporator

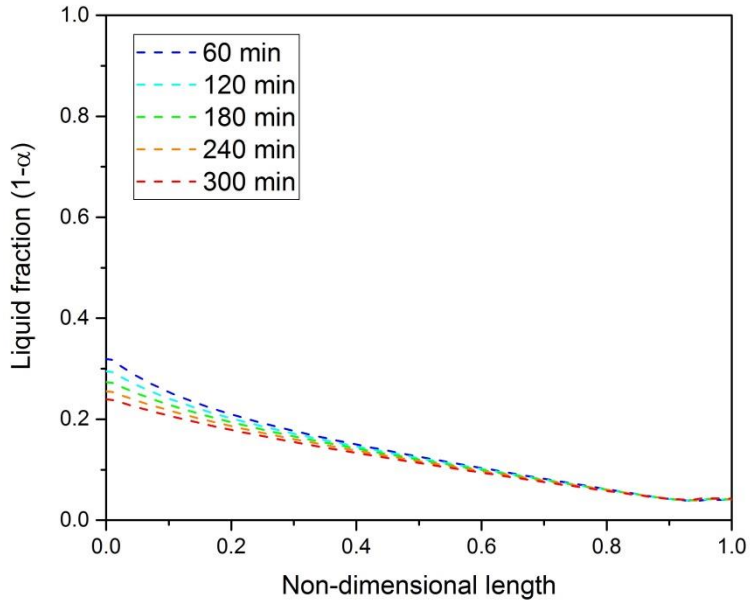

Figure 6.6 (b) Liquid fraction curves in the evaporator

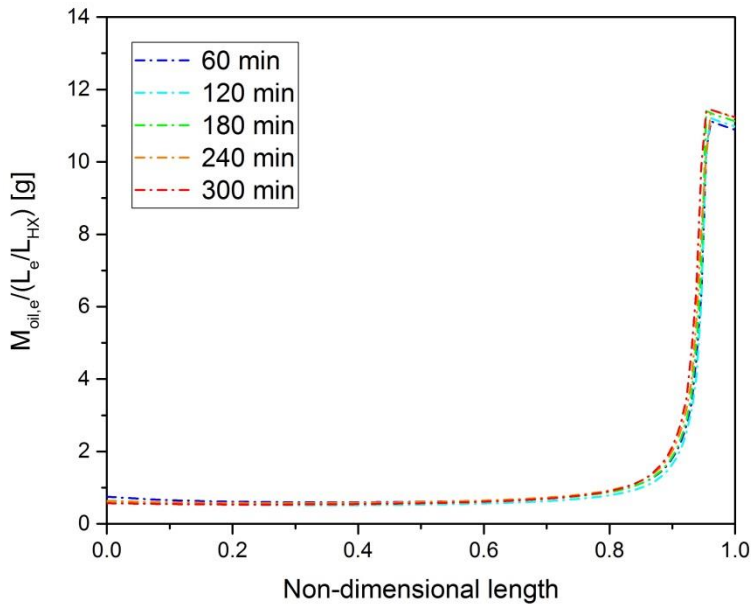

Figure 6.6 (c) Local distribution of oil in the evaporator

One common observation in both Figure 6.5 and 6.6 is, the oil retention is generally higher at the superheated region. In Chapter 4, it has been explained by the smaller liquid velocity at this region. To prove that, the average liquid velocity in the evaporator at t=60 min is potted in Figure 6.7.

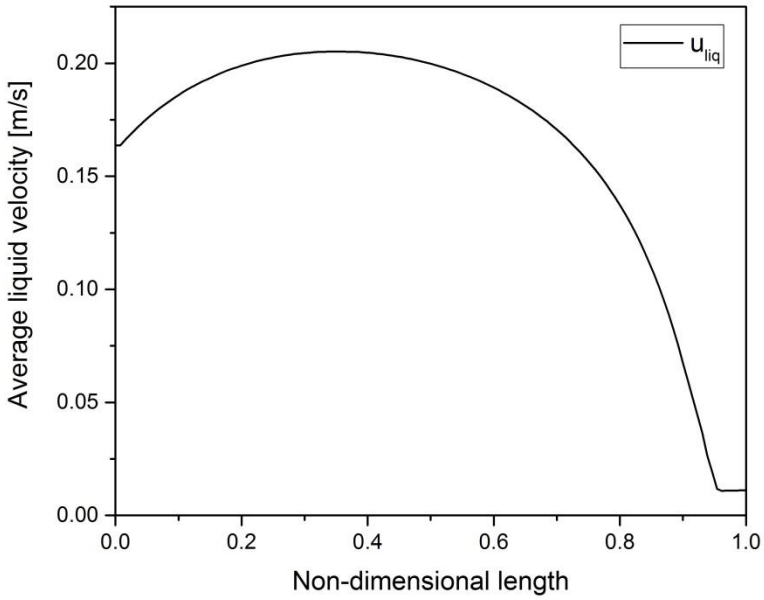

Figure 6.7 Average liquid velocity in the evaporator at t=60 min

Figure 6.7 shows clearly the average liquid velocity is much lower in the superheated region. It also reveals that the oil is more likely retained at the location where the liquid velocity is low. This validates the analysis in the Chapter 4.

CHAPTER 7-SUMMARY AND CONCLUSIONS

7.1 Conclusions from Experimental Study

In summary, the transient refrigerant and oil mass distribution are measured in each component of a residential heat pump water heater (HPWH) unit. R134a is used to pair with POE 22 oil as the working fluid. The conclusions of the current experimental work are summarized as follows:

- Quick Closing Valve Technique (QCVT) is employed to localize the refrigerant and oil into each component in the system; Remove and Weigh Technique (RWT) is then used to measure the refrigerant mass, with an uncertainty about 0.17% of the total refrigerant charge; the retained oil mass in each component, except for the compressor, is mainly determined by Mix and Sample Technique (MST), of which the uncertainty is about 0.15% of the total oil charge.
- Most of the refrigerant is distributed in two heat exchangers and the liquid line due to either a large internal volume or a high refrigerant density. During the heating process, the refrigerant inventory increases in the condenser due to a higher subcooling, and decreases in the evaporator because of a higher inlet quality.
- Only less than 4% of oil escapes from the compressor during the 5 hours' heating. Most of the escaped oil is retained in two heat exchangers and the accumulator. The oil retention increases with time in the evaporator; in the condenser, it decreases first then increases. These transient variations are caused by the changes in the liquid refrigerant-oil mixture velocity.

7.2 Conclusions from System Performance Model

A linked EES-CFD system model has been developed to simulate the transient system performance of the HPWH during the heating process. The influence of oil on the system performance is neglected in the modeling due to a relatively small OCR (<0.3%) during the heating process. The conclusions of the system modeling are as follows:

- Compared with the experiential data, this linked EES-CFD system model predicts the system capacities and power with an average deviation of 4.2%. The

deviations in the prediction of the water temperatures are within 4^{o}C.

- A higher deviation can be observed at the later stage of the heating. This may be because the Boussinesq approximation used in the CFD model will deviate from the reality if the stratification of water temperature is too intensive.

7.3 Conclusions from Retention Model of Heat Exchangers

A retention model has been developed to predict the refrigerant and oil inventory in the heat exchangers. This model uses the results of the system modeling. Mixture thermal properties are considered. Main conclusions for this modeling are:

- The average error of the prediction of refrigerant retention in the condenser and evaporator is 9.9% and 15.2% respectively. The model underestimates the retention in both heat exchangers, but it successfully captures the transient change of the refrigerant retention in the heat exchangers.
- The deviation in the prediction of oil retention is much larger. The average difference between measured data and modeling results for the condenser and evaporator is 57.5% and 51.6% respectively. Besides, it gives a different trend of oil retention in the condenser, compared with the experiments.
- Oil tends to be retained in the superheated region due to a lower liquid velocity. In this region, the oil retention is high sensitive to the liquid fraction. The inaccuracy of the void fraction model might explain the large deviation in the oil retention prediction

REFERENCES

[1] G. F. Hewitt. *Measurement of Two Phase Flow Parameters.* Academic Press Inc., 1978.

[2] E. Björk. A simple technique for refrigerant mass measurement. *Applied Thermal Engineering*, 25(8-9):1115-1125, 2005.

[3] N. Tanaka, M. Ikeuchi, and G. Yamanaka. Experimental study on the dynamic characteristics of a heat pump. *ASHRAE Transactions*, 88(2):323-331, 1982.

[4] W. J. Mulroy and D. A. Didion. Refrigerant migration in a split-unit air conditioner. *ASHRAE Transactions*, 91(1A):193-206, 1985.

[5] M. R. Hoehne and P. S. Hrnjak. Charge minimization in systems and components using hydrocarbons as a refrigerant. *Technical Report ACRC TR-224*, University of Illinois at Urbana-Champaign, 2004.

[6] S. Peuker and P. Hrnjak. Experimental and analytical investigation of refrigerant and lubricant migration. *Technical Report ACRC TR-277*, University of Illinois at Urbana – Champaign, 2010.

[7] S. Jin and P. Hrnjak. Distribution of refrigerant and lubricant in automotive air condition systems. *Technical Report ACRC TR-291*, University of Illinois at Urbana University of Illinois at Urbana-Champaign, 2012.

[8] L. Jiang and P. Hrnjak. Refrigerant charge reduction in small commercial refrigeration systems, *Technical Report ACRC TR-310*, University of Illinois at Urbana - Champaign, 2014.

[9] W. A. Miller. The laboratory evaluation of the heating mode part-load operation of an air-to-air heat pump. *ASHRAE Transactions*, 91(2B):524-536, 1985.

[10] M. I. Belth, T. E. Grzymala and D. R. Tree. Transient mass-flow rate of a residential air-to-air heat-pump. *International Journal of Refrigeration*, 11(5):298-304, 1988.

[11] V. P. Sheth and T. A. Newell. Refrigerant and oil migration and retention in air conditioning and refrigeration systems. *Technical Report ACRC TR-224*, University of Illinois at Urbana-Champaign, 2005.

[12] E. Björk and B. Palm. Refrigerant mass charge distribution in a domestic refrigerator. Part I: Transient conditions. *Applied Thermal Engineering*, 26(8-9):829-837, 2006.

[13] T. A. Shedd and T. A. Newell. Automated optical liquid film thickness measurement method, *Review of Scientific Instruments*, Vol. 69, No. 12, 4205-4213, 1998.

[14] J.P. Lee. experimental and theoretical investigation of oil retention in carbon dioxide air-conditioning system, Ph.D. Thesis, CEEE, University of Maryland, College Park, MD, 2002.

[15] L. Cremaschi. Experimental and theoretical investigation of oil retention in vapor compression systems, Ph.D. Thesis, CEEE, University of Maryland, College Park, MD, 2004.

[16] J. A. Crompton, T. A. Newell, and J. C. Chato. Experimental measurement and modeling of oil holdup. *Technical Report ACRC TR-226*, University of Illinois at Urbana-Champaign, 2004.

[17] S. A. Klein. EES – Engineering Equation Solver.

[18] J. T. Brebner and A. T. Welford. Introduction: an historical background sketch. In A. T. Welford (Ed.), Reaction Times. Academic Press, New York, pp. 1-23, 1980.

[19] T. Shah and P. Hrnjak. Linked Modelling of Heat Pump Water Heater Vapor Compression System and Water Tank. *International Refrigeration and Air Conditioning Conference at Purdue,* Paper 1481, Purdue University, IN, 2014.

[20] D. M. Staley, C. W. Bullard and R. R. Crawford. Steady-State Performance of a Domestic Refrigerator/Freezer Using R12 and R134a. *Technical Report ACRC TR-022,* University of Illinois at Urbana-Champaign, 1992.

[21] F. D. Incropera and D. P. DeWitt. Fundamentals of heat and mass transfer, fifth edition. Wiley, 2002.

[22] C. Wang, K Chi and C Chang. Heat transfer and friction characteristics of plain fin-and-tube heat exchangers, part II: Correlation. *International Journal of Heat and Mass Transfer,* 43, 2693-2700, 2009.

[23] V. Gnielinski. New equations for heat and mass transfer in turbulent pipe and channel flow, *International Chemical Engineering,* Vol. 16, No. 2, pp. 359-368, 1976.

[24] J. P. Wattelet, J. C. Chato, B. R. Christoffersen, et al. Heat transfer flow regimes of refrigerants in a horizontal-tube evaporator. *Technical Report ACRC TR-055*, University of Illinois at Urbana-Champaign, 1994.

[25] S. W. Churchill. Friction-factor equation spans all fluid flow regimes, *Chemical Engineering*, No. 7, pp.91-92, 1977.

[26] A. L. Souza and M. M. Pimenta. Prediction of pressure drop during horizontal two-phase flow of pure and mixed refrigerants, *ASME Conf. Cavitation and multiphase flow*, FED-vol. 210, pp.161-171, 1995

[27] S.Z. Rouhani and E. Axelsson. Calculation of void volume fraction in the sub cooled and quality boiling regions. *International Journal of Heat and Mass Transfer,* 13, 383–393, 1970.

[28] M. K. Dobson and J. C. Chato, Condensation in smooth horizontal tubes, *Journal of Heat Transfer*, 120:2, pp.193-213, 1998.

[29] D. Henderson. Solubility, viscosity and density of refrigerant/lubricant mixtures. The Air-Conditioning and Refrigeration Technology Institute. Rep. DOE/CE/23810-34, 1994.

[30] M. K. Jensen and D. L. Jackman. Prediction of nucleate pool boiling heat transfer coefficients of refrigerant-oil mixtures, *Trans. of ASME, Journal of Heat Transfer*, Vol. 106: 184-190. 1984.

[31] C. J. Seeton, CO2-lubricant two-phase flow patterns in small horizontal wetted wall channels; the effects of refrigerant/lubricant thermophysical properties. PhD dissertation, University of Illinois at Urbana-Champaign, 2009.

[32] J. Xiao and P. Hrnjak. A new flow regime map and void fraction model based on the flow characterization of condensation. *International Journal of Heat and Mass Transfer,* 108,443-452, 2017.

APPENDIX A: ORIGINAL DATA

Table A-1 Charge Tests

Charge [g]	Q_{cr} [kW]	Q_{er} [kW]	COP
755	1.51	1.16	3.54
772.5	1.50	1.14	3.53
793.5	1.56	1.20	3.58
813.5	1.57	1.21	3.60
823.5	1.53	1.18	3.57
833.5	1.50	1.16	3.54
855.5	1.52	1.16	3.56

Table A-2 System performance

Time [min]	Q_{cr} [kW]	Q_{er} [kW]	Q_{comp} [kW]	COP	$T_{w,v}$ [^{o}C]	$T_{w,ht}$ [^{o}C]	$T_{w,hb}$ [^{o}C]
0	0.00	0.00	0.00	0.00	25.0	24.9	25.1
5	1.55	1.37	0.40	3.87	25.4	25.5	25.1
10	1.57	1.32	0.40	3.91	25.7	26.2	25.0
15	1.58	1.30	0.40	3.95	26.2	26.9	25.2
20	1.61	1.30	0.40	4.01	26.7	27.3	25.6
25	1.58	1.27	0.40	3.96	27.0	27.8	26.0
30	1.59	1.26	0.40	3.95	27.5	28.2	26.5
35	1.62	1.28	0.40	4.05	28.0	28.4	27.1
40	1.62	1.27	0.40	4.02	28.5	29.2	27.5
45	1.61	1.26	0.40	4.02	28.9	29.6	28.0
50	1.60	1.25	0.40	3.97	29.3	29.9	28.4
55	1.62	1.27	0.41	4.00	29.7	30.3	29.0
60	1.60	1.25	0.40	3.97	30.1	30.8	29.3
65	1.60	1.25	0.41	3.92	30.6	31.4	29.8
70	1.60	1.24	0.41	3.90	31.1	32.0	30.2
75	1.62	1.26	0.41	3.94	31.5	32.1	30.8
80	1.58	1.23	0.41	3.84	31.9	32.7	31.0
85	1.60	1.24	0.41	3.89	32.3	33.0	31.6
90	1.60	1.24	0.41	3.85	32.7	33.4	32.0
95	1.58	1.23	0.41	3.82	33.1	34.0	32.4
100	1.60	1.24	0.42	3.84	33.5	34.3	33.0
105	1.60	1.24	0.42	3.81	34.0	34.7	33.4
110	1.59	1.22	0.42	3.76	34.5	35.1	33.8
115	1.61	1.24	0.42	3.79	34.9	35.8	34.3

Table A-2 (cont.)

120	1.61	1.24	0.43	3.76	35.3	36.2	34.8
125	1.61	1.23	0.42	3.78	35.8	36.6	35.1
130	1.56	1.19	0.43	3.63	36.2	36.8	35.6
135	1.56	1.22	0.43	3.65	36.6	37.3	36.1
140	1.60	1.25	0.43	3.75	37.0	37.9	36.5
145	1.64	1.25	0.43	3.77	37.4	38.4	36.9
150	1.57	1.21	0.44	3.56	37.9	38.8	37.3
155	1.51	1.17	0.43	3.52	38.2	39.1	37.7
160	1.56	1.22	0.44	3.57	38.6	39.7	38.1
165	1.63	1.25	0.44	3.72	39.1	39.9	38.7
170	1.57	1.19	0.44	3.55	39.5	40.5	39.0
175	1.58	1.19	0.45	3.54	39.9	40.8	39.6
180	1.58	1.19	0.45	3.50	40.4	41.1	39.9
185	1.57	1.18	0.45	3.49	40.6	41.4	40.3
190	1.59	1.20	0.45	3.51	41.2	41.7	40.7
195	1.55	1.17	0.46	3.39	41.5	42.7	41.0
200	1.56	1.17	0.45	3.44	42.0	42.9	41.4
205	1.57	1.18	0.45	3.45	42.4	43.2	41.9
210	1.54	1.15	0.46	3.34	42.7	43.9	42.2
215	1.57	1.18	0.46	3.41	43.2	43.9	42.8
220	1.57	1.17	0.46	3.41	43.7	44.3	43.2
225	1.57	1.17	0.46	3.39	44.0	44.7	43.6
230	1.55	1.16	0.47	3.33	44.4	45.4	43.8
235	1.55	1.15	0.47	3.31	44.9	45.8	44.3
240	1.54	1.15	0.47	3.28	45.4	46.2	44.7
245	1.53	1.13	0.47	3.24	45.7	46.7	45.2
250	1.54	1.14	0.48	3.23	46.1	46.9	45.7
255	1.52	1.13	0.47	3.21	46.6	47.4	46.1
260	1.56	1.14	0.47	3.29	46.8	47.6	46.4
265	1.53	1.12	0.48	3.18	47.2	48.3	46.7
270	1.52	1.12	0.48	3.15	47.8	48.7	47.2
275	1.56	1.13	0.49	3.18	48.2	48.7	47.7
280	1.51	1.11	0.49	3.11	48.4	49.5	48.0
285	1.52	1.11	0.49	3.08	48.9	49.7	48.5
290	1.51	1.10	0.49	3.09	49.1	50.3	48.7
295	1.50	1.10	0.49	3.04	49.6	50.6	49.1
300	1.52	1.10	0.49	3.08	50.1	50.7	49.6

Table A-3 Measurements of internal volume

Section	Liquid Ref. Method [cc]	Isothermal Gas Method [cc]
Condenser	970.4	973.3
Liquid line	147.7	157.0
Evaporator	568.1	549.1
Accumulator	285.0	275.5
Compressor	2992.4	2969.7

Table A-4 Verification tests of the Mix and Sample Technique (MST)

Oil charged [g]	Oil measured [g]
5.2	5.6
10.5	10.9
20.7	20.8
29.6	29.8
1.2	1.0

Table A-5 Distribution of refrigerant [g]

Time [min.]	Evap.	Cond.	Accum.	liquid line	Comp.	Total measured	Original charge
60	117.9	471.6	5.6	163.5	55.8	814.4	817.1
120	119.0	473.5	6.5	169.1	54.3	822.3	818.1
180	114.5	462.3	5.7	172.1	52.4	807.1	812.1
240	99.6	482.4	5.6	170.4	50.7	808.7	812.6
300	106.6	478.6	5.7	168.3	57.0	816.1	814.0

Table A-6 Distribution of oil [g]

Time [min.]	Evap.	Cond.	Accum.	liquid line	Comp.	Total measured	Original charge
60	2.4	3.8	2.5	0.5	264.2	273.4	273.8
120	2.7	3.5	2.4	0.4	265.8	274.9	273.2
180	2.8	2.7	2.7	0.5	267.7	276.3	275.2
240	3.3	3.1	2.0	0.5	268.2	277.1	276.2
300	3.6	3.5	2.5	0.4	261.7	271.7	273.3